IMPROVED TECHNIQUES FOR THE DECOMPOSITION OF HOT-WIRE FLUCTUATION MEASUREMENTS IN SUPERSONIC FLOWS

By

CHIN-LONG KO

Bachelor of Engineering
Chung Yuan Christian College
of Science and Engineering
Chung Li, Taiwan
1970

Master of Science
Oklahoma State University
Stillwater, Oklahoma
1974

Submitted to the Faculty of the Graduate College
of the Oklahoma State University
in partial fulfillment of the requirements
for the Degree of
MASTER OF SCIENCE
May, 1976

IMPROVED TECHNIQUES FOR THE DECOMPOSITION OF HOT-WIRE FLUCTUATION MEASUREMENTS IN SUPERSONIC FLOWS

Thesis Approved:

Dennis K McLaughlin
Thesis Adviser

W. G. Tiederman

Ladislaus J Fila

Dean of the Graduate College

PREFACE

This work originated from the need to provide a reliable interpretation of hot-wire anemometer fluctuation measurements in the supersonic jet noise research performed at Oklahoma State University. The objective of this work was to develop a data reduction technique which included hot-wire end-loss corrections to determine the mass velocity fluctuations and total temperature fluctuations in a supersonic turbulent flow field.

I am deeply indebted to Professor Dennis K. McLaughlin for suggesting this research and his guidance, encouragement and patience during this period of study. I wish also to thank my other committee members, Professor Ladislaus J. Fila and Professor William G. Tiederman for their advice and guidance. Appreciation is also expressed to Mr. Gerald L. Morrison and Mr. Timothy R. Troutt for their help in experiments and their invaluable discussions and careful checking of derivations and data reductions.

I would also like to express my sincere appreciation to the entire faculty at the School of Mechanical and Aerospace Engineering, OSU for their guidance and financial support with a graduate assistantship. I am very grateful for my parents whose understanding and support made my graduate study possible.

TABLE OF CONTENTS

LIST OF TABLES

LIST OF FIGURES

NOMENCLATURE

$A_{(\ )}$	fluctuation sensitivity in constant temperature operation
a_w	overheating parameter, $\frac{R_w - R_r}{R_r}$
$B_{(\ )}$	fluctuation sensitivity in constant current operation
C	thermal capacity of wire
CCA	constant current hot-wire anemometer
CTA	constant temperature hot-wire anemometer
C_p	specific heat of fluid at constant pressure
D	diameter of nozzle
d	diameter of hot-wire
E	bridge voltage
E_w	voltage across wire
e'	fluctuating voltage across wire
$\tilde{e}$	r.m.s. voltage across wire nondimensionalized with the mean voltage
I	current
K	total conduction heat transfer rate
k_o	thermal conductivity of air at stagnation temperature
ℓ	wire length
M	local Mach number
M_j	Mach number at jet exit
m	mass velocity
m_o	parameter, $d\ell nu_o / d\ell nT_o$

Nu_o	Nusselt number based on k_o
n_o	parameter, $d\ell nk_o/d\ell nT_o$
P	local static pressure
P_o	stagnation pressure
Q	total convection heat transfer rate
R	gas constant
R_a	resistance of bridge resistor in CCA
R_B	resistance of bridge resistor in CTA
R_b	bridge null resistance of CCA
Re	jet Reynolds number
Re_o	local Reynolds number, $\frac{\rho ud}{\mu_o}$
R_L	lead resistance
R_{mTo}	correlation coefficient between fluctuations of the mass velocity and total temperature
R_{uT}	correlation coefficient between velocity and temperature fluctuations
R_w	wire resistance
$R_{\rho u}$	correlation coefficient between density and velocity fluctuations
$R_{\rho T}$	correlation coefficient between density and temperature fluctuations
r	parameter, A_m/A_T
r'	parameter, B_m/B_T
T	local temperature
T_o	stagnation temperature
T_r	recovery temperature
T_{ref}	reference temperature

T_w wire temperature

t time

u velocity

x,y,z rectangular coordinates

Z_s finite impedance of circuit as seen from hot-wire terminals in CCA

α $1/\{1 + [(\gamma - 1) / 2] M^2\}$

α_1 resistance temperature coefficient of wire

β $(\gamma - 1) M^2 \alpha$

γ ratio of specific heats (1.40 for present study)

ε total conduction heat transfer ratio

ρ density

λ finite circuit factor of CCA

η recovery factor, T_r/T_o

Π sound pressure mode amplitude

Θ overheating parameter, T_w/T_o

σ entropy mode amplitude

τ vorticity mode amplitude

τ_w temperature loading, $\dfrac{T_w - T_r}{T_o}$

τ_{wr} overheat ratio, $\dfrac{T_w - T_r}{T_r}$

ϕ yaw angle of wire relative to local flow angle

μ viscosity

μ_o viscosity at stagnation temperature

Superscripts

$( )'$ fluctuating quantity

$\overline{(\ )}$ time-averaged quantity

$\tilde{(\ )}$ r.m.s. fluctuating quantity nondimensionalized with the mean value

$(\ )'_{rms}$ root-mean-square fluctuating quantity

CHAPTER I

INTRODUCTION

The hot-wire anemometer is a major diagnostic instrument in high speed aerodynamics. It has been a useful tool in understanding the structure and characteristics of turbulence which cannot be predicted by purely theoretical considerations. Kovasznay (6, 7, 8) and Morkovin (14, 15) pioneered the problem of the interpretation of hot-wire signals in supersonic flow by extending the low-speed hot-wire techniques to high-speed compressible flows.

The interpretation of hot-wire signals is based on the analysis of the heat transfer from the hot-wire to the surrounding fluid. This analysis can be complicated when a substantial portion of the heat transfer from the wire is conduction to the hot-wire supports. This conduction end-loss becomes increasingly important as the local hot-wire Reynolds number is decreased. The ratio of conduction heat transfer to total heat transfer from the hot-wire (ε) is typically in the range from 30% to 90% for a local hot-wire Reynolds number of $Re_o = 5$ to $Re_o = 30$. The value of ε depends on the characteristics of the wire, the overheat loading, and the flow conditions over the wire.

In supersonic flows, in order to avoid wire breakage, it is usually necessary to operate the hot-wire in low density air with the local wire Reynolds number (Re_o) less than 50. Therefore, in almost every case of high speed hot-wire anemometry, the conduction end-loss is significant.

Dewey (4) and Lord (12) have analyzed the end-loss problem in the measurement of mean flow properties in supersonic flows. However, a systematic technique for correcting for the hot-wire end-loss error in the measurement of fluctuating quantities has not yet been reported in the open literature.

Experimenters, following Morkovin (14) and Morkovin and Phinney (15) have normally calibrated the fluctuation sensitivities (at least in part) for individual wires in a way which eliminates some major errors in the final data (10, 17, 18). However, because these methods do not explicitly deal with the end-loss, significant errors in the final data can result. (The size of these errors is strongly dependent on the details of the experiment.) This point will be more thoroughly discussed later.

The purpose of this work was to develop a reliable technique for correcting the end-loss error for the hot-wire fluctuation measurements in supersonic flows. The analysis and data reduction techniques are presented for use with both constant temperature hot-wire anemometers (CTA) and constant current anemometers (CCA).

In theory, the end-loss problem can be avoided by completely calibrating each hot-wire used in the measurements. Demin and Zheltukhin (3) employed this direct-sensitivity technique on the basis that it is practically impossible to allow for such phenomena as contamination, oxidation, and other individual features of the hot-wire theoretically. However, this direct-sensitivity technique is also practically unreasonable, because it is so time consuming. (A full calibration of this nature typically takes several hours during which time small shifts in the hot-wire properties are almost unavoidable.) This led Rose (18) to attempt a semi-calibration method by calibrating the sensitivity of mass velocity

fluctuations directly and calculating the sensitivity of stagnation temperature fluctuations from Morkovin's theory (14). However, we believe the stagnation temperature fluctuation sensitivities given by this technique are inaccurate because of the non-uniform application of the effective end-loss calibration. Our technique accounts for the end-loss in a systematic and uniform way, and hence, avoids the major source of error in the hot-wire measurements.

To test the reliability of our data reduction techniques numerous hot-wire fluctuation measurements were made in the highly turbulent portions of two supersonic jets (M_j = 2.4 and M_j = 1.5). These measurements were performed on several days with different hot-wires and with the two sets of hot-wire electronics (the constant current anemometer [CCA] and the constant temperature anemometer [CTA]). The probe locations of this investigation are on the center-line of the jet nine nozzle diameters downstream from the jet exit and on the shear annulus of the jet at both five and nine nozzle diameters downstream from the jet exit. Kovasznay mode diagrams are obtained as the main vehicle for comparison of the results.

CHAPTER II

METHOD OF APPROACH

There are two types of hot-wire anemometers in general use: the constant temperature anemometer and the constant current anemometer. Although the computations involved for each type are different from each other, the basic theories can be derived from a general analysis based on the energy balance of the hot-wire. In this approach, it is assumed that the hot-wire is operated in a supersonic flow field with local Mach number being greater than 1.3. The techniques will not be applied to transonic flow because of the additional complication of Mach number dependence on several parameters such as Nusselt number and recovery factor.

Hot-Wire Bridge Circuits

The constant current anemometer (CCA) was developed first (6) and has been used more extensively for supersonic hot-wire turbulence measurements (15). Referring to a schematic diagram in Figure 1 (see Appendix C), a simple series circuit is constructed consisting of a current supply (batteries), a large current controlling variable resistor R_d, a variable bridge null resistor R_b, bridge resistors R_a and R_c, some measuring devices and the hot-wire. The bridge is set to balance by varying the bridge null resistor R_b such that the wire resistance R_w and lead resistance R_L become

$$R_w + R_L = \frac{R_a R_b}{R_c}$$

The wire current and voltage across B_1 and B_2 are measured. Since the current controlling resistor R_d is many times larger than the hot-wire resistance, small changes in the hot-wire resistance (caused by variation in heat transfer due to the turbulence) have negligible variation on the current in the circuit.

The constant temperature anemometer (CTA) development has been greatly enhanced by advances in solid state micro circuitry. Referring to a schematic diagram in Figure 2, the essential ingredient in the anemometer is the control circuit and the feedback amplifier K controls the bridge current so that the resistance of hot-wire is maintained at a constant value within a very close tolerance (despite rapid changes in heat transfer from the wire). The feature which enables the operator to set a desired hot-wire overheat and traverse the probe to various positions in flowfield without concern for burning out the wire is very convenient.

Theoretical Analysis

The energy equation for a hot-wire being operated in a flow field is:

$$I^2 R_w = Q + K + C \frac{dT_w}{dt} \tag{2.1}$$

where Q is the rate of total convection heat transfer from the overheated hot-wire to the surrounding fluid flow, K is the rate of total conduction heat transfer from the wire to both supports and CdT_w/dt is the rate of energy change of the wire.

During a measurement with the constant temperature anemometer the last term in the equation is negligible and is neglected in our analysis. In constant current operation the last term (known as the thermal inertia term) has a significant effect. It causes the hot-wire response to

decrease with increasing frequency of the flow fluctuations. Since the decreasing frequency response is identical to that of a first order system it can be corrected for by using a compensated amplifier, which is an essential ingredient in all CCA sets. With a compensated amplifier the accuracy of the amplifier output voltage and its relationship to the flow fluctuations is strongly dependent on the accuracy with which the break frequency (or time constant) of the amplifier is set.

Assuming the thermal inertia term is either negligible as in the CTA or taken care of by the compensation amplifier in the CCA the heat balance becomes

$$I^2 R_w = Q + K \tag{2.2}$$

Using ohms law, the left hand side can be expressed as $\frac{E_w^2}{R_w}$. Following Kovasznay (6, 7) and Morkovin (14) the convection heat transfer rate can be expressed as

$$Q = \pi \ell \; k_o \; (T_w - T_r) \; Nu_o \tag{2.3}$$

where k_o and Nu_o are the thermal conductivity of the fluid and the mean Nusselt number which are based on the stagnation temperature of the flow T_o (7). T_w and T_r are the mean wire temperature and the mean wire recovery temperature, respectively. (For a complete list of nomenclature refer to page viii.) By introducing the recovery factor

$$\eta = \frac{T_r}{T_o} \tag{2.4}$$

Equation (2.3) can also be expressed as

$$Q = \pi \ell \; k_o \; (T_w - \eta T_o) \; Nu_o \tag{2.5}$$

Following Morkovin (14), we can reasonably assume that Nu_o and η are functions of a few non-dimensional quantities. Assuming constant Prandtl

number fluid flow, the functional relationships for a normal hot-wire are as follows:

$$Nu_o = f(Re_o, M, \Theta) \tag{2.6}$$

$$\eta = g(Re_o, M) \tag{2.7}$$

where Re_o is the local Reynolds number

$$Re_o = \frac{\rho\, ud}{\mu_o} \tag{2.8}$$

and μ_o is the viscosity at the local stagnation temperature T_o. θ is the ratio of the wire temperature to the stagnation temperature of the flow.

$$\theta = \frac{T_w}{T_o} \tag{2.9}$$

If the hot-wire is oriented with a yawed angle ϕ in the stream, the parameter ϕ should be included in the nondimensional groups of Equations (2.6) and (2.7) (see Morkovin and Phinney [15]).

In the interpretation of hot-wire fluctuation signals the local linearization concept, first introduced by Kovasznay (7) is used. This involves identifying the fluctuating portion of the hot-wire voltage, the velocity, the fluid density and the stagnation temperature with differentials in the quantities: i.e., $e' = dE$, $u' = du$, $\rho' = d\rho$ and $T_o' = dT_o$. Using this linearization $\frac{e'}{E} = \frac{dE}{E} = d \ln E$. Hence, to obtain the relationship between the hot-wire voltage fluctuation term e'/E and the fluctuations in the flow quantities we follow the procedure of Morkovin (14) and logarithmically differentiate Equation (2.2). This yields:

$$2d\ell n\, E_w - d\ell n\, R_w = (1 - \varepsilon)\, d\ell n\, Q + \varepsilon\, d\ell nK \tag{2.10}$$

where

$$\varepsilon = \frac{K}{K + Q}$$

To determine the derivative of the total convection term $d\ell nQ$, we can logarithmically differentiate Equation (2.5) as follows

$$d\ell nQ = d\ell nk_o + d\ell nT_o + d\ell n\tau_w + d\ell nNu_o \tag{2.11}$$

where

$$\tau_w = \frac{T_w - T_r}{T_o}$$

The terms $d\ell n\tau_w$ and $d\ell nNu_o$ can be further expanded by employing Equations (2.6), (2.7) and the following relations

$$d\ell nRe_o = d\ell n\rho + d\ell nu - d\ell n\mu_o \tag{2.12}$$

$$d\ell nM = \frac{1}{\alpha}\,(d\ell nu - \tfrac{1}{2}\, d\ell nT_o) \tag{2.13}$$

where

$$\alpha = \frac{1}{(1 + \frac{\gamma - 1}{2} M^2)}$$

Furthermore, the following parameters can also be defined as in Morkovin (14).

$$n_o = \frac{d\ell nk_o}{d\ell nT_o} \tag{2.14}$$

$$m_o = \frac{d\ell n\mu_o}{d\ell nT_o} \tag{2.15}$$

$$\tau_{wr} = \frac{T_w - T_r}{T_r} \tag{2.16}$$

n_o and m_o depend upon the stagnation temperature only and can be taken as constants, specifically 0.885 and 0.765 for stagnation temperatures between 270°K and 350°K.

By employing the above relations, Equation (2.10) can be further expanded in terms of its logarithmic partial derivatives in the flow quantities and hot-wire operating temperature in a manner similar to Morkovin (14):

$$2d\ell nE_w - d\ell nR_w = (1-\varepsilon)\left[\frac{\partial \ell nNu_o}{\partial \ell nRe_o} + \frac{1}{\alpha}\frac{\partial \ell nNu_o}{\partial \ell nM} - \frac{1}{\tau_{wr}}\left(\frac{1}{\alpha}\frac{\partial \ell n\eta}{\partial \ell nM} + \frac{\partial \ell n\eta}{\partial \ell nRe_o}\right)\right]$$

$$d\ell nu + (1-\varepsilon)\left[\frac{\partial \ell nNu_o}{\partial \ell nRe_o} - \frac{1}{\tau_{wr}}\frac{\partial \ell n\eta}{\partial \ell nRe_o}\right] d\ell np + (1-\varepsilon)$$

$$\left[\frac{1}{\tau_{wr}}\left(\frac{1}{2\alpha}\frac{\partial \ell n\eta}{\partial \ell nM} + m_o\frac{\partial \ell n\eta}{\partial \ell nRe_o}\right) + n_o - \frac{1}{\tau_{wr}} - \left(\frac{1}{2\alpha}\frac{\partial \ell nNu_o}{\partial \ell nM} + m_o\frac{\partial \ell nNu_o}{\partial \ell nM} + \right.\right.$$

$$\left.\left.\frac{\partial \ell nNu_o}{\partial \ell n\Theta}\right)\right] d\ell n T_o + \left[(1-\varepsilon)\left(\frac{\partial \ell nNu_o}{\partial \ell n\Theta} + 1 + \frac{1}{\tau_{wr}}\right) + \varepsilon\frac{d\ell n K}{d\ell nT_w}\right]$$

$$d\ell nT_w \qquad (2.17)$$

Equation (2.17) is valid for operations using normal wires with both constant temperature and constant current anemometers. The additional term ε which is the ratio of the conduction heat transfer rate K to the total heat transfer rate makes this equation differ from Morkovin's equation (14). (If ε is set = 0 the equation reduces to Morkovin's equation).

In order to reduce the complexity of the analysis, the conduction heat transfer rate has been taken to be a function of only the temperature of the wire and the mean flow parameters. Hence, we neglect fluctuations in the support temperature and in the instantaneous spatial temperature profile of the wire. The simplifying assumptions are reasonable because (i) the relatively large hot-wire supports have enough thermal inertia to prevent them from following temperature fluctuations in the flow, (ii) the approximation of negligible change in the temperature profile of the wire is consistent with the local linearization assumption which is made following Kovasznay (6) and Morkovin (14) later and which is a fundamental principle in this hot-wire work.

Constant Temperature Hot-Wire Anemometry

In constant temperature operation, the wire resistance R_w and the hot-wire temperature T_w are held constant by the electronics. Therefore, Equation (2.17) reduces to:

$$\frac{dE_w}{E_w} = \frac{(1 - \varepsilon)}{2}\left[\frac{\partial \ell nNu_o}{\partial \ell nRe_o} + \frac{1}{\alpha}\frac{\partial \ell nNu_o}{\partial \ell nM} - \frac{1}{\tau_{wr}}\left(\frac{1}{\alpha}\frac{\partial \ell n\eta}{\partial \ell nM} + \frac{\partial \ell n\eta}{\partial \ell nRe_o}\right)\right]\frac{du}{u} +$$

$$\frac{(1 - \varepsilon)}{2}\left[\frac{\partial \ell nNu_o}{\partial \ell nRe_o} - \frac{1}{\tau_{wr}}\frac{\partial \ell n\eta}{\partial \ell nRe_o}\right]\frac{d\rho}{\rho} + \frac{(1 - \varepsilon)}{2}\left[\frac{1}{\tau_{wr}}\left(\frac{1}{2\alpha}\frac{\partial \ell n\eta}{\partial \ell nM} + m_o\frac{\partial \ell n\eta}{\partial \ell nRe_o}\right) + n_o - \frac{1}{\tau_{wr}} - \left(\frac{1}{2\alpha}\frac{\partial \ell nNu_o}{\partial \ell nM} + m_o\frac{\partial \ell nNu_o}{\partial \ell nRe_o} + \frac{\partial \ell nNu_o}{\partial \ell n\Theta}\right)\right]$$

$$\frac{dT_o}{T_o} \qquad (2.18)$$

Since the voltages being measured from the constant temperature anemometers are the bridge voltages, we should convert the voltage across the wire to the bridge voltage by

$$E_w = \frac{R_w}{R_w + R_L + R_B} E_B \qquad (2.19)$$

where R_L is the lead resistance and R_B is the resistance of the resistor in the bridge which is always a constant. Taking the logarithmic derivative of Equation (2.19), yields

$$d\ell nE_w = d\ell nE_B + \frac{R_L + R_B}{R_w + R_L + R_B} d\ell nR_w \qquad (2.20)$$

since the wire resistance is held constant for the constant temperature set, Equation (2.20) becomes

$$\frac{dE_w}{E_w} = \frac{dE_B}{E_B} \qquad (2.21)$$

Hence, Equation (2.18) can be applied directly to the decomposition of bridge voltage without making any modifications.

Besides identifying the fluctuating quantities with the differentials of the quantities, for example $e' = dE$, the local linearization implies that fluctuations in the hot-wire voltage can be represented as:

$$\frac{e'}{\overline{E}} = A_u \frac{u'}{\overline{u}} + A_\rho \frac{\rho'}{\overline{\rho}} - A_T \frac{T_o'}{\overline{T}_o} \tag{2.22}$$

This says that the instantaneous voltage fluctuation is caused by fluctuations in velocity, density and total temperature and the sensitivities to the individual flow fluctuations are A_u, A_ρ and A_T. (The sign conventions used is convenient since all sensitivities are then positive definite quantities). Comparing Equation (2.22) with Equation (2.18), we can determine the sensitivity coefficients to be:

$$A_u = \frac{(1-\varepsilon)}{2}\left[\frac{\partial \ell n Nu_o}{\partial \ell n Re_o} + \frac{1}{\alpha}\frac{\partial \ell n Nu_o}{\partial \ell n M} - \frac{1}{\tau_{wr}}\left(\frac{1}{\alpha}\frac{\partial \ell n \eta}{\partial \ell n M} + \frac{\partial \ell n \eta}{\partial \ell n Re_o}\right)\right] \tag{2.23}$$

$$A_\rho = \frac{(1-\varepsilon)}{2}\left[\frac{\partial \ell n Nu_o}{\partial \ell n Re_o} - \frac{1}{\tau_{wr}}\frac{\partial \ell n \eta}{\partial \ell n Re_o}\right] \tag{2.24}$$

$$A_T = \frac{(1-\varepsilon)}{2}\left[\frac{1}{\tau_{wr}} - n_o - \frac{1}{\tau_{wr}}\left(\frac{1}{2\alpha}\frac{\partial \ell n \eta}{\partial \ell n M} + m_o \frac{\partial \ell n \eta}{\partial \ell n Re_o}\right) + \left(\frac{1}{2\alpha}\frac{\partial \ell n Nu_o}{\partial \ell n M} + m_o \frac{\partial \ell n Nu_o}{\partial \ell n Re_o} + \frac{\partial \ell n Nu_o}{\partial \ell n \Theta}\right)\right] \tag{2.25}$$

Examination of the velocity and density fluctuation sensitivities reveals that they differ only by terms involving logarithmic differentiation with respect to Mach number. Because of the Mach number independence principle, these derivatives are approximately zero for Mach numbers greater than 1.3. (This is well-substantiated by experimental evidence (1, 15)). As a consequence $A_u = A_\rho = A_m$ where

$$A_m = \frac{(1-\varepsilon)}{2}\left[\frac{\partial \ell n Nu_o}{\partial \ell n Re_o} - \frac{1}{\tau_{wr}}\frac{\partial \ell n n_o}{\partial \ell n Re_o}\right] \tag{2.26}$$

And A_T reduces to

$$A_T = \frac{(1-\varepsilon)}{2}\left[\frac{1}{\tau_{wr}} - n_o + \frac{\partial \ell n Nu_o}{\partial \ell n \theta}\right] + m_o A_m \tag{2.27}$$

and

$$\frac{e'}{E} = A_m \frac{(\rho u)'}{\overline{\rho u}} - A_T \frac{To'}{\overline{T_o}} \tag{2.28}$$

Although this is a major simplification, it unfortunately insures that decomposing the velocity fluctuations and density fluctuations from the mass velocity fluctuations $(\rho u)'$ is in general impossible without making an ad hoc assumption concerning the form of the fluctuations present in the flow.

Our voltage fluctuation detectors always detect the mean square voltage fluctuations (or rms fluctuations); hence following Kovasznay (7, 8) we write:

$$\frac{\overline{e'^2}}{\overline{E}^2 A_T^2} = \frac{\tilde{e}^2}{A_T^2} = \tilde{m}^2 r^2 - 2R_{mTo}\,\tilde{m}\tilde{T}_o r + \tilde{T}_o^2 \tag{2.29}$$

where $r = \frac{A_m}{A_T}$; $\tilde{m} = \frac{(\rho u)'_{rms}}{\overline{\rho u}}$, $\tilde{T}_o = \frac{(T_o)'_{rms}}{\overline{T_o}}$

and $R_{mTo} = \frac{\overline{(\rho u)' To'}}{(\rho u)'_{rms} (T_o)'_{rms}}$

Hence, if the sensitivities A_m and A_T are determined from mean flow data then, for each measurement of $\tilde{e}$, there are three unknown quantities: $\tilde{m}$, $\tilde{T}_o$ and R_{mTo}. Theoretically, these quantities can be determined by measuring $\tilde{e}$ at three different wire overheat conditions and simultaneously solving the three equations for the three unknowns. In actual practice, experimental uncertainties amplify to such an extent in this

procedure that accurate results are very difficult to obtain particularly for the quantities $\tilde{T}_o$ and R_{mTo}. Consequently, many measurements are usually made and the resulting $\tilde{e}/A_T$ quantities are plotted as a function of r. These diagrams have become known as Kovasznay mode diagrams following Kovasznay's pioneering work (7, 8).

It is important to understand that for any given flow position, the shape of the Kovasznay mode diagram, the $\tilde{e}/A_T$ intercept, and the slope at large values of r are all dependent only on the properties of the flow. Hence, measurements with different sensors (or different hot-wire electronics) should yield identical mode diagrams for one position in the flow, provided the A_m and A_T sensitivities for each sensor are properly determined.

As we will show in the Results chapter, we have also plotted several of our 'mode' diagrams in Morkovin coordinates which are $\tilde{e}/A_\sigma$ versus A_τ/A_σ where A_σ is the sensitivity to entropy fluctuations and A_τ is the sensitivity to vorticity fluctuations (14). Our data interpretation is typically enhanced by doing this.

The detailed procedure we follow in determining our hot-wire fluctuation sensitivities A_m and A_T is thoroughly discussed in Chapter III. However, it is important to make a few points concerning the procedure at this stage. All of the logarithmic derivatives in Equations (2.26) and (2.27) are determined from infinite length wire calibration data (1, 4, 20). Hence, with knowledge of the hot-wire overheat ratio (from experimentally determined resistance-temperature relationships) the only remaining unknown is ε, the ratio of conduction heat transfer rate to total heat transfer rate.

We have used two methods to determine ε. One method is to perform

a vaccuum calibration together with a mean flow calibration of a typical wire and use Lord's procedure (12) to compute ε. Under vacuum conditions the only heat transfer from the wire is conduction to the supports. Lord has developed a systematic technique to use this information to accurately predict the mean conduction heat transfer rate for the probe in the flow field. The other method for determining ε follows the technique of both Rose (18) and Demin and Zheltukhin (3) in directly calibrating A_m from mean flow calibration data as follows:

$$A_m = \frac{\overline{\rho u}}{\overline{E}} \frac{\partial \overline{E}}{\partial (\overline{\rho u})} \Bigg|_{\overline{T}_o = \text{const},\ R_w = \text{const}} \tag{2.30}$$

Because this sensitivity A_m is directly calibrated for each hot-wire it must include the effect of end-losses and hence is equivalent to the A_m of Equation (2.26). Thus, as mentioned in the introduction, Rose's hot-wire decomposition technique does in part account for the end-loss which is so important in many flow situations.

Although the direct-sensitivity calibration technique can be extended to the total temperature fluctuation sensitivity

$$A_T = \frac{\overline{T}_o}{\overline{E}} \frac{\partial \overline{E}}{\partial \overline{T}_o} \Bigg|_{\overline{\rho u} = \text{const},\ R_w = \text{const}} \tag{2.31}$$

following Demin and Zheltukhin (3), the resulting calibration procedure is considerably more time consuming. (It also required precise control over the stagnation temperature of the flow field. The stilling chamber stagnation temperature of our facility is always atmospheric temperature; hence we do not have the necessary control to use the procedure of Demin and Zheltukhin.) Consequently, we use an alternate procedure in which A_m is directly calibrated, but A_T is calculated from Equation (2.27)

after ε has been determined. We determine ε from the calibrated A_m and infinite length wire heat transfer data using Equation (2.26) rearranged as:

$$\varepsilon = 1 - \frac{2A_m}{\left[\frac{\partial \ell n Nu_o}{\partial \ell n Re_o} - \frac{1}{\tau_{wr}} \frac{\partial \ell n \eta}{\partial \ell n Re_o}\right]} \tag{2.32}$$

We should add at this point that we have made several comparisons of ε determined from our procedure using Equation (2.32) with those determined using Lord's (12) vacuum calibration procedure and the results are always within the estimated uncertainties of our measurements. Consequently, we use the method we have devised (Equation 2.32) because it is easier and more direct in the present application.

Constant Current Hot-Wire Anemometry

The data reduction procedure for constant current anemometry is significantly different from the CTA case. Since the temperature of the hot-wire is not held constant in the CCA operation, $d\ell nR_w$ and $d\ell nT_w$ will not be zero in Equation (2.17). However, instead

$$d\ell nR_w = d\ell nE_w \tag{2.33}$$

and

$$d\ell nT_w = \frac{d\ell nT_w}{d\ell nR_w} \, d\ell nE_w \tag{2.34}$$

As noted by Morkovin (14), the actual current in a "constant current" system is not truly constant when resistance variations are induced by the flow because of the finite impedance Z_s of the circuit feeding the hot-wire. Thus, a parameter λ which includes the sympathetic variation between R_w and I is introduced.

i.e., $$\lambda = -\frac{\partial \ell nI}{\partial \ell nR_w} = -\frac{R_w}{I}\frac{\partial I}{\partial R_w} \tag{2.35}$$

Including the parameter λ, the logarithmic variation of the wire resistance and wire temperature becomes

$$d\ell nR_w = \frac{1}{(1-\lambda)} d\ell nE_w \tag{2.36}$$

$$d\ell nT_w = \frac{1}{(1-\lambda)} \frac{d\ell nT_w}{d\ell nR_w} d\ell nE_w \tag{2.37}$$

The parameter λ can be determined from the ratio between the mean voltage drop across the wire, E_w, and the battery voltage for series current control, since

$$\lambda = \frac{R_w}{Z_s + R_w} \tag{2.38}$$

Usually λ is a very small quantity (on the order of 0.003) and, hence, it can be neglected without introducing significant error.

Rearrangement of Equation (2.17) with the substitution of Equations (2.36) and (2.37) and the approximations $\lambda \simeq 0$ and all derivatives with respect to Mach number are approximately zero yields:

$$\left[1 - (1-\varepsilon)\frac{d\ell nT_w}{d\ell nR_w}\left(1 + \frac{1}{\tau_{wr}} + \frac{\partial \ell nNu_o}{\partial \ell n\Theta}\right) - \frac{d\ell nK}{d\ell nR_w}\right]\frac{dE_w}{E_w} = (1-\varepsilon)$$

$$\left[\frac{\partial \ell nNu_o}{\partial \ell nRe_o} - \frac{1}{\tau_{wr}}\frac{\partial \ell n\dot{m}}{\partial \ell nRe_o}\right]\frac{d(\rho u)}{(\rho u)} + (1-\varepsilon)\left[m_o - \frac{1}{\tau_{wr}} - m_o\right.$$

$$\left.\left(\frac{\partial \ell nNu_o}{\partial \ell nRe_o} - \frac{1}{\tau_{wr}}\frac{\partial \ell n\,\eta}{\partial \ell nRe_o}\right) - \frac{\partial \ell nNu_o}{\partial \ell n\Theta}\right]\frac{dT_o}{T_o} \tag{2.39}$$

Employing the local linearization concept as introduced previously, yields:

$$\frac{e'}{E} = -B_m\frac{(\rho u)'}{\rho u} + B_T\frac{T_o'}{T_o} \tag{2.40}$$

where

$$B_m = \frac{(1-\varepsilon)}{2B_e}\left[\frac{\partial \ell nNu_o}{\partial \ell nRe_o} - \frac{1}{\tau_{wr}}\frac{\partial \ell n\,\eta}{\partial \ell nRe_o}\right] \tag{2.41}$$

$$B_T = \frac{(1-\varepsilon)}{2B_e}\left[-n_o + \frac{1}{\tau_{wr}} + \frac{\partial \ell n Nu_o}{\partial \ell n \Theta}\right] + m_o B_m \tag{2.42}$$

And B_e is defined to be

$$B_e = \frac{(1-\varepsilon)}{2}\left(1 + \frac{1}{\tau_{wr}} + \frac{\partial \ell n Nu_o}{\partial \ell n \Theta}\right)\frac{d\ell n T_w}{d\ell n R_w} + \frac{\varepsilon}{2}\frac{d\ell n K}{d\ell n R_w} - \frac{1}{2} \tag{2.43}$$

Note that the sensitivities of constant current operation can be related to the sensitivities of constant temperature operation as follows:

$$B_\rho = \frac{A_\rho}{B_e} \tag{2.44}$$

$$B_m = \frac{A_m}{B_e} \tag{2.45}$$

$$B_T = \frac{A_T}{B_e} \tag{2.46}$$

Again, the r.m.s. mass velocity fluctuation and r.m.s. total temperature fluctuation can be obtained in the same way as in constant temperature operation. Equation (2.40) can be manipulated to give an equation similar to Equation (2.29).

$$\frac{\tilde{e}^2}{B_T^2} = \tilde{m}^2 r'^2 - 2R_{mTo}\,\tilde{m}\tilde{T}_o\, r' + \tilde{T}_o^2 \tag{2.47}$$

where

$$r' = \frac{B_m}{B_T}$$

As indicated before, the Kozasznay mode diagram or our modification thereof can also be plotted after determining $\tilde{e}/B_T$ and r' at several distinct current levels for a point in the flow. Then the mass velocity fluctuations $\tilde{m}$, the total temperature fluctuations $\tilde{T}_o$, and their correlation coefficient R_{mTo} can be obtained in a manner similar to CTA operation. Again it is important to emphasize that the quantitative slope of the mode diagram is dependent solely on the properties of the flow. Comparisons between CCA and CTA mode diagrams should yield identical

results, within the uncertainties of the measurements.

As in the CTA case, the sensitivity to mass velocity fluctuations B_m can be determined from a mean flow calibration as follows:

$$B_m = \left. \frac{-\overline{\rho u}}{\overline{E}} \frac{\partial \overline{E}}{\partial (\overline{\rho u})} \right|_{\overline{T}_o = \text{const}, \; I = \text{const}.} \tag{2.48}$$

However, the end-loss ratio ε cannot be determined directly from this, as we did in the CTA case with Equation (2.32), since the term B_e contains an unknown logarithmic derivative of the end-loss $\frac{d\ell nK}{d\ell nR_w}$.

Hence, the most appropriate technique to use to determine ε is the Lord vacuum calibration procedure (12). In fact, because of the peculiarity of our Flow Corporation CCA electronics, which make it inconvenient to run a constant current level calibration, it is actually more convenient and more accurate to determine B_m from Equation (2.41) using our vacuum calibrated ε and infinite-wire logarithmic derivatives for the other terms (1, 4, 20). B_T is determined, analogously to A_T, by using Equation (2.42) and ε and the logarithmic derivatives as above.

CHAPTER III

EXPERIMENTAL CONSIDERATIONS

Experimental Apparatus

The experiments were performed in the Oklahoma State University free jet test facility. Schematic diagrams are shown in Figure 3 and Figure 4 (see Appendix C). Two axisymmetric supersonic de Laval nozzles with exit Mach numbers of 2.4 and 1.5 (exit diameters 9.52 mm and 7.90 mm respectively) were used in this study.

The jet facility is operated by evacuating its downstream section with a Kinney vacuum pump. It also enables the vacuum calibration of hot-wire conduction to be performed. The inlet to the jet is a 15 cm diameter stilling section. A thermocouple was employed in this section to measure the stagnation temperature and a pressure tap to measure stagnation pressure. To reduce the turbulence levels upstream of the nozzle a 5 cm section of foam rubber and six fine screens are located in the stilling section. The contraction ratio in the stilling chamber is over 200 to one.

In order to avoid the significant humidity effects on the Mach number, compressed air from a high pressure compressor with chemical dryers was used. The Reynolds number of the flow can be varied by adjusting the stagnation pressure P_o, upstream of the nozzle. The pressure in the test chamber is controlled by a variable area exit diffuser and

maintained within 1% of the nozzle exit pressure. The probes are mounted on a three degree of freedom probe drive which can locate the probe within $\pm$0.1 mm.

Both constant temperature and constant current anemometers were used in this study. The constant temperature anemometer is a DISA 55M01 set and the constant current anemometer is a Flow Corporation HWB-3 battery-operated set. The hot-wire probes are made from DISA 55A53 subminiature probes epoxied to the upper edge of brass stems. The diameter of the wire (platinum plated tungsten) is five microns and the distance between the supports is about one mm. Hence, the aspect ratio for these wires is about 200. Some of the hot-wire probes were modified by spreading the prongs approximately 1.5 mm apart and soldering new 5μm wire in place as before. These wires had an aspect ratio of about 300 and subsequently lower end-loss ratios.

A Multimetrics model AF 120 active band pass filter was employed to filter frequencies below 1KHz from the hot-wire signal in order to eliminate low frequency oscillations characteristic of the vacuum chamber. The upper frequency cutoff was set at 20,000 Hertz which in all cases was lower than the frequency response limitation at the lowest overheat ratio of the CTA. (Frequency response decreases drastically with decreasing overheat ratio and decreasing local Reynolds number for the CTA.) Hence, the bandpass filter always controlled the frequency range of the fluctuations being measured, and not the anemometer electronics. The resulting mode diagrams do not have complicated frequency response dependence.

It is important to point out that McLaughlin, et al. (13) have shown that the dominant portion of the fluctuation energy is below 20 KHz for

the M_j = 2.4 jet, and they have subsequently determined that this is also true for the M_j = 1.5 jet in the Reynolds number range of the present experiments. It should also be noted that for the limited number of higher Reynolds number experiments (Re = 75,000 at M_j = 2.4) the CTA hot-wire frequency response exceeded 50 KHz even at an overheat ratio a_w of only 10% ($a_w = (R_w - R_r)/R_r$). Thus, the modal decomposition techniques using the present method with commercial CTA electronics can be applied to a wide variety of supersonic flows, provided sufficient caution is taken in evaluating the instrumentation frequency response capabilities.

Both anemometers used in this study have built in square wave generators which are used to evaluate the upper frequency response limitations of the respective electronics and hot-wire probe combinations.

Experimental Procedure and Data Reduction

This study concentrated on evaluating the mass velocity fluctuations and the total temperature fluctuations at the central position and on the shear annulus of the free jet nine nozzle diameters downstream from the nozzle exit and the shear layer of this jet five nozzle diameters downstream from the nozzle exit. The probe position on the shear annulus is chosen to be the radial location of maximum hot-wire voltage fluctuations. The free stream stagnation pressures P_o were set at about 12 and 24 inches of mercury which correspond to free stream Reynolds numbers based on the nozzle diameter of about 37,000 and 75,000 for the free stream Mach number M_j = 2.4 jet. P_o was set at about nine inches of mercury which corresponds to a free stream Reynolds number based on the

nozzle diameter of about 33,000 for the free stream Mach number M_j = 1.5 jet.

Mean flow hot-wire calibrations yielded data such as that shown in Figure 5 for CTA operation. These measurements were performed with the hot-wire placed at the exit of the nozzle on the centerline of the jet. Previous pitot pressure and static pressure probe measurements had accurately established the Mach number of the flow at that point. Logarithmic slopes at various positions on these curves provide the mass velocity fluctuation sensitivities A_m for various wire overheat and mean flow conditions. The mean mass velocity $\overline{\rho u}$ at a general position in the flowfield is determined from a measurement of $\overline{E}$, and calibration curves which have been slightly modified by interpolation to produce lines of constant overheat ratio (rather than constant wire resistance as in Figure 5). By doing this, the modified calibration data, as shown in Figure 6 (Appendix C) can be used to determine the $\overline{\rho u}$ at a position in the flow which has a value of T_o different from the T_o value at the calibration position.

In CCA operations the mean flow calibration curves look typically like those presented in Figure 7. As we mentioned in Chapter II, it was more convenient and more accurate to determine B_m from Equation (2.41) having previously determined ε from Lord's vacuum calibration technique, rather than take the logarithmic slopes of the data of Figure 7. This is because the data of Figure 7 has been obtained from several cross plots, each one of which introduce additional uncertainty. The cross plotting is necessary because our CCA electronics is operated for specific bridge resistance ratios, rather than specific set of currents. Other CCA electronic sets do not have this peculiar set up.

The evaluation of the wire temperature, the recovery temperature and the overheat ratio τ_{wr} were based on the assumption that the variation of resistance against temperature is linear, i.e.,

$$T_w = T_{ref} + \frac{R_w - R_{ref}}{\alpha_1 R_{ref}} \tag{3.1}$$

where R_{ref} and T_{ref} are the reference resistance and reference temperature of the wire and α_1 is the temperature coefficient of the wire which is approximately 0.004 per degree Kelvin for tungsten wire. (The exact value is determined by calibration for each probe.)

In order to estimate the variation of Nusselt number Nu_o and recovery factor η with respect to their independent variables, the universal data calibrated by several hot-wire investigators were employed (1, 20). Behrens (1) suggested the following empirical relation for the recovery factor η in terms of Re_o.

$$\eta = 1.167 - \frac{0.217}{1 + \frac{1}{(0.335\ Re_o)^{1.33}}} \tag{3.2}$$

which fits experimental data well for $M > 1.3$. Dewey (4) reported the calibrated data for the variation of Nusselt number Nu_o with respect to Re_o and the variation of Nu_o with respect to the overheat ratio τ_{wr}. Vrebalovich (20) has given the following relations to determine the variation of Nu_o with respect to Re_o for an infinite length wire with zero overheat:

$$Nu_o = 0.00268\ Re_o^2 - 0.0313\ Re_o^{3/2} + 0.154\ Re_o + 0.0423\ Re_o^{\frac{1}{2}} - 0.00528 \tag{3.3a}$$

for $M \geq 1.2$ and $Re_o < 16$

and $Nu_o = -0.52 + 0.457\ \sqrt{Re_o}$

for $M \geq 1.2$ and $Re_o \geq 16$ (3.3b)

The logarithmic derivatives of η and Nu_o were obtained by differentiating Equations (3.2) and (3.3).

To estimate the local Mach number at the point of interest, it is assumed that the local static pressures are the same as the chamber pressures measured and the following relation can be derived from the ratio of stagnation to static temperature, the ideal gas law, and the relationship between acoustic velocity and temperature:

$$M = \left[\frac{-1 + \sqrt{1 + \frac{2(\gamma-1)}{\gamma} \frac{(\rho u)^2 RT_o}{P^2}}}{(\gamma - 1)} \right]^{1/2} \qquad (3.4)$$

The local stagnation temperatures were determined from measurements of hot-wire recovery resistances and the evaluation of recovery factors from Equation (3.2). The estimated stagnation temperature will be an approximation, since the recovery factor determined from Equation (3.2) is the recovery factor for infinite length wire, however, it has only very small effect in determining local wire Reynolds number Re_o and Mach number.

Frequency response plays an important role in the fluctuation voltage measurements. The CCA has a compensation amplifier to compensate for the lack of frequency response. The compensation frequency setting which effects the amplifier gain was determined by using the standard square wave technique discussed by Kovasznay (7).

A summary of the important steps and the order of these steps in the data reduction procedures is presented in Appendix B.

Presentation of Results

As discussed in Chapter II the major results of our hot-wire fluctuation measurements are presented in the form of Kovasznay (8) mode diagrams which are plots of the coordinates $\tilde{e}/A_T$ versus A_m/A_T (or $\tilde{e}/B_T$ versus B_m/B_T for CCA operation). As discussed in Chapter II and as will be shown in the next chapter on results, the output parameters from this type of mode diagram are $\tilde{m}$, $\tilde{T}_o$ and R_{mTo}.

In most cases we are more interested in the velocity fluctuation $\tilde{u}$ in preference to the mass velocity fluctuation $\tilde{m}$. There are two established procedures for obtaining $\tilde{u}$ data, both procedures in practice requiring an assumption concerning the form of the fluctuating parameters.

For shear flows with a large amount of velocity fluctuations it is common practice (5, 10, 14, 17, 19) to assume that the pressure fluctuations are negligible in comparison with the fluctuations in velocity, density and temperature. With this assumption the following relationships can be derived for the computations of the velocity, temperature and density fluctuations:

$$\tilde{u}^2 = \frac{1}{(\alpha + \beta)^2} \left[\tilde{T}_o^2 + 2\alpha R_{mTo} \tilde{m}\tilde{T}_o + \alpha^2 \tilde{m}^2 \right] \tag{3.5}$$

$$\tilde{T}^2 = \tilde{\rho}^2 = \frac{1}{(\alpha + \beta)^2} \left[\tilde{T}_o^2 - 2\beta R_{mTo} \tilde{m}\tilde{T}_o + \beta^2 \tilde{m}^2 \right] \tag{3.6}$$

$$R_{uT}\tilde{u}\tilde{T} = \frac{1}{(\alpha + \beta)^2} \left[\tilde{T}_o^2 + (\alpha - \beta) R_{mTo} \tilde{m}\tilde{T}_o - \alpha\beta\tilde{m}^2 \right] \tag{3.7}$$

where

$$\alpha = \frac{1}{1 + \frac{(\gamma - 1)}{2} M^2}$$

$$\beta = (\gamma - 1) M^2 \alpha$$

An alternate approach in modal decomposition has been proposed by Morkovin (14) and used most recently by Laderman and Demetriades (10). Morkovin (14) further decomposed the hot-wire signals into three fluctuation modes as pressure fluctuations Π, entropy fluctuations σ, and vorticity fluctuations τ which are defined as follows:

$$\Pi = \frac{p'}{\gamma \bar{p}} \tag{3.8a}$$

$$\sigma = \frac{s'}{Cp} \tag{3.8b}$$

$$\tau = \frac{u'}{\bar{u}} \tag{3.8c}$$

By decomposing the hot-wire signals into these three fluctuation modes, Equation (2.22) becomes:

$$\frac{e'}{\bar{E}} = -A_\sigma \sigma - A_\tau \tau - A_\Pi \Pi \tag{3.9}$$

where

$$A_\sigma = A_m + \alpha A_T$$

$$A_\tau = \beta A_T - A_m$$

$$A_\Pi = \alpha(\gamma - 1)\, A_T - A_m$$

Morkovin has demonstrated that if the pressure fluctuations are negligible then temperature and velocity fluctuations can be determined directly from a new mode diagram which is a plot of $\tilde{e}/A_\sigma$ versus A_τ/A_σ. In the present work some example Morkovin mode diagrams are presented along with their resulting predictions of the fluctuations. In all cases the fluctuations predicted in this way are in good agreement with those obtained from the Kovasznay mode diagrams and the use of Equations (3.5), (3.6) and (3.7).

CHAPTER IV

EXPERIMENTAL RESULTS

Experimental Determination of Fluctuation Sensitivities

Before presenting the fluctuation measurements it is appropriate to show the experimental data which is used to determine the fluctuation sensitivities.

As indicated previously, the mass velocity sensitivities A_m were evaluated from direct calibrations which also determine the conduction end-loss ratios indirectly for CTA operations. Hence, great attention should be paid to the reliability of the calibrations.

Figure 8 (see Appendix C) shows mean flow calibration data for the CTA with the same hot-wire probe but with two different Mach numbers. From the similar shape and slopes of the curves one can expect that the logarithmic derivatives of these curves have the same dependence on overheat ratio, and the Mach number independence is verified in this case. The uniform shape of the curves is also a measure of repeatability of our instrumentation.

The vacuum calibration plays an important role in determining conduction end-loss ratios ε in CCA operations. To examine the consistency in these calibrations, results from calibrations with the same hot-wire probe on different days are shown in Figure 9 (see Appendix C). Typical variations of the conduction end-loss ratio ε against the overheat ratio τ_{wr} for both CCA and CTA operations are shown in Figure 10 (see Appendix

C). Typical variations of mass velocity fluctuation sensitivities and total temperature fluctuation sensitivities versus the overheat resistance ratio in CTA operations and CCA operations are shown in Figures 11 and 12 (see Appendix C), respectively.

The determination of compensation frequency is very important in the measurement of r.m.s. fluctuation voltage in the CCA operations. Figure 13 (Appendix C) shows that compensation frequencies of CCA system decrease with increasing overheat ratios which also implies that the time constants decrease with decrease of overheat ratios. In contrast to this feature, time constants of CTA system usually increase with decrease of overheat ratios (Figure 14, Appendix C). Notice that the slowest time response of the CTA system shown on Figure 14 (Appendix C) is 6.5 μsec which corresponds to an upper frequency cutoff of 24.5 KHz. Since we are measuring fluctuations in the 1 to 20 kHz frequency band, the CTA has adequate frequency response, and no compensation is required in its case.

Fluctuation Mode Diagram Results

Several experiments with different hot-wire probes and different anemometers were made in order to evaluate the reliability of present data reduction schemes. The consistency in results obtained from experiments run on different days with different anemometers and hot-wire probes with different aspect ratios provides an indication of the reliability of our techniques. A summary of the pertinent details is shown in Table I for these experiments.

Figure 15 (Appendix C) shows an example mode diagram (in Kovasznay coordinates, 8) which was obtained in the Mach number 2.4 jet, with the probe positioned nine diameters downstream from the exit on the shear layer (SL) where the hot-wire fluctuations are maximum. The cross

TABLE I

SUMMARY OF FLOW AND PROBE CONDITIONS FOR EXPERIMENTS

Date	Anemo-meter	Probe			Jet Properties		Local Properties	
		Identi-fication	Aspect Ratio	Position	M_j	Re	M	Re_o
5/30/75	CTA	F	300	X/D = 9, CL*	2.4	35,200	2.3	8.8
6/11/75	CTA	I	300	X/D = 9, CL	2.4	41,100	2.3	10.1
7/3/75	CCA	I	300	X/D = 9, CL	2.4	35,600	2.3	8.7
7/10/75	CTA	I	300	X/D = 9, CL	1.5	31,000	1.1	9.4
				X/D = 5, SL*	1.5	31,500	1.4	12.4
8/11/75	CTA	I	300	X/D = 5, Y/D = .487	2.4	38,500	1.2	4.1
				X/D = 5, Y/D = .454	2.4	38,300	2.1	8.6
				X/D = 5, Y/D = .440	2.4	38,700	2.4	10.8
				X/D = 9, SL	2.4	37,700	1.3	4.1
8/13/75	CCA	I	300	X/D = 5, SL	2.4	36,300	2.2	8.4
				X/D = 9, SL	2.4	35,800	1.4	4.1
8/28/75	CCA	I	300	X/D = 9, CL	1.5	34,000	1.3	11.8
				X/D = 5, SL	1.5	32,800	1.4	13.2
9/11/75	CTA	H	200	X/D = 9, CL	2.4	36,100	2.4	10.1
					2.4	74,100	2.4	18.9
				X/D = 5, SL	2.4	36,000	2.0	7.9
					2.4	72,900	2.1	15.6
				X/D = 9, SL	2.4	36,100	1.5	5.2
					2.4	72,800	1.4	9.4

*CL indicates the centerline location of the jet.

*SL indicates the shear layer of the jet which is determined as maximum fluctuation position.

symbols represent data which have been reduced using the present procedure with the end-loss correction. Shown on the same figure is data which have been reduced by the partial calibration technique suggested by Rose (18). Although the details of the CTA versus CCA operation preclude a generalization on the matter, several investigators appear to have used a somewhat similar technique to Rose (10, 17, 22). This entails determining A_m (or B_m) from direct calibration or from calibrated Nu_o and η dependence on Re_o, and then determining A_T (or B_T) by an equation similar to Equation (2.27) with ε set to zero.

The striking feature of the data of Figure 15 (Appendix C) is that the individual data points plot very differently for the present data reduction technique compared with the previous technique of Rose (18). The raw data used with both techniques was identical. Hence we expect a large effect in our calculated quantities, particularly $\tilde{T}_o$ and R_{mTo}. The $\tilde{m}$ values for the two sets of data are very similar ($\tilde{m}$ is equal to the slope of the curve at large values of r). The reason for this is most certainly because the mass velocity fluctuation sensitivities A_m of the two data reduction methods are identical.

The data of Figure 15 (Appendix C) is rather an extreme case since the Reynolds number is low (Re_o = 5.2) and the aspect ratio of the wire is only 200. Hence, the end-loss ratio is typically high as shown in Figure 16 (Appendix C) as a function of wire overheat ratio. Shown on the same plot is $(1-\varepsilon)$ which represents the fraction of the heat loss which is convection, and hence represents the portion of the heat loss from which the flow properties are determined. In many flow situations investigated by previous researchers the end-losses would have been much less than those shown here (11, 12, 15).

The flow fluctuations $\tilde{m}$ and $\tilde{T}o$ and their correlation coefficient R_{mTo} are determined from the data plotted on the Kovasznay mode diagram (for example, Figure 15, Appendix C). From Equation (2.29) we see that the mode diagram is a second order polynomial in $(\tilde{e}/A_T)^2$ versus r coordinates or a hyperbola in $(\tilde{e}/A_T)$ versus r coordinates. Consequently, we obtain the best estimate of the mode diagram from the individual data points by using a method of least squares to fit a hyperbola to the $\tilde{e}/A_T$ versus r data. This procedure is discussed more thoroughly in Appendix A.

An evaluation of our present method of data reduction is performed in two ways. First, the analysis must be reasonable and self-consistent. Second, mode diagrams made with both the CTA and CCA anemometers as well as with probes of different aspect ratios can be compared for consistency. Figure 17 (see Appendix C) presents such comparison data for the data points first presented in Figure 15. Included on the plot are the estimated experimental uncertainty bands for both the CTA data as well as the CCA data. The constant current anemometer data has generally wider uncertainty bands which are primarily attributed to the uncertainty in setting the compensation time constant with the square wave technique. In view of the experimental uncertainties we conclude that the mode diagrams resulting from the CTA and from the CCA are in good agreement and our confidence in the reliability of our technique is enhanced.

Also shown on Figure 17 (see Appendix C) is the hyperbola which we obtained from a least square regression technique outlined in Appendix A for the September 11, 1975 data. No attempt was made to curve fit the CCA data since the uncertainty bands are so much larger that our confidence in the data is less. We should point out that the uncertainty

bands on our CCA data may be unduely large because we are using a rather old anemometer (Flow Corporation Model HWB-3). Newer models have more sophisticated electronics which may provide higher accuracy in the measurements. However, even in these models the uncertainty in the data is caused primarily by the uncertainty in the time constant setting.

Mode diagrams for two other positions in the flow are shown in Figures 18 and 19 (Appendix C). Overall, the agreement between the CTA data and the CCA data is very good. The data of Figure 18 at a probe location of X/D = 5 on the edge of the jet shows a degree of inconsistency between the three sets of CTA data which is greater than the data of the other two probe locations. We have attributed the discrepency to our inability to position the probe at exactly the same position on the very thin shear layer. At nine diameters downstream the shear layer is much thicker and our positioning resolution is much better.

Experiments were also performed at several positions in the M_j = 2.4 jet at a jet Reynolds number more than twice the jet Reynolds number for the previous data. The major objective of this experiment was to find the behavior of the end-loss ratio ε with changing Reynolds number. Figure 20 (Appendix C) shows the experimentally determined end-loss ratios ε as a function of overheat ratio τ_{wr} for the probe positioned at X/D = 5 on the shear layer (solid symbols). The low Reynolds number data for the same probe position, and the same probes are shown on the figure with open circles. This data displays the feature of increasing end-loss with decreasing Reynolds number that one would expect. We have also included with open square symbols data obtained at this position using a probe with a much larger aspect ratio (around 300). This probe displays a smaller end-loss again, as one would expect. One

further word is in order concerning the shape of these curves. At zero overheat ratio the convection heat transfer is approximately zero and hence the end-loss ratio should go to 1 (ref. Lord, 12). The data shown in Figure 20 (Appendix C) is consistent with this fact.

The mode diagram corresponding to the probe position on the shear layer five diameters downstream of the exit at high Re is shown in Figure 21 (See Appendix C). Included on the figure is the low Reynolds number mode diagram for comparison. As we sould expect for a nearly fully turbulent flow, there is very little Reynolds number dependence in the phenomenon being measured.

Presented in Table II are the flow fluctuation data $\tilde{m}$, $\tilde{T}_o$ and R_{mTo} corresponding to the mode diagrams previously shown (Figures 17, 18, 19 and 21, Appendix C). These parameters have all been obtained from curves generated by the least squares regression fit of a hyperbola to the data accumulated by all the CTA experiments at the respective flow position. In three cases, all of which are discussed in Appendix A, we applied a minor adjustment to the parameters $\tilde{T}_o$ and/or R_{mTo} in order to constrain the solutions to be physically reasonable.

The mass velocity fluctuations $\tilde{m}$ are all high enough to confirm the fact that the flow is turbulent (however, it may be in the final stages of transition from laminar flow). The fluctuations are the highest at nine diameters downstream of the exit on the edge of the jet. More thorough surveys of ours indicate that this is near the end of the potential core of the jet.

The total temperature fluctuations $\tilde{T}_o$ are in all cases less than 3% which is expected since the jets are unheated and hence, the mean flow is approximately isoenergetic ($\overline{T}_o \simeq$ constant).

TABLE II

ESTIMATED MASS VELOCITY FLUCTUATIONS, TOTAL TEMPERATURE FLUCTUATIONS AND THEIR CORRELATION COEFFICIENTS IN THE $M_j = 2.4$ JET

Probe Position	Figure	$\tilde{m}$	$\tilde{T}_o$	R_{mTo}
X/D = 9, SL	17	0.252	0.029	0.618
X/D = 5, SL *	18	0.189	0.012	1.000
X/D = 9, CL *	19	0.171	0.000	--
X/D = 5, SL; R_e = 72,900	21	0.217	0.024	0.977

* The values obtained are determined from averaging of all the CTA data.

Because the total temperature fluctuations are so small in comparison with the mass velocity fluctuations they cannot be determined as accurately as can $\tilde{m}$. For the measurements reported here we have estimated uncertainties in $\tilde{m}$ to be $\pm$ 0.03 (which is $\pm$ 15% of typical $\tilde{m}$) compared with uncertainties in $\tilde{T}_o$ of approximately $\pm$ .01 (which is $\pm$ 100% of a typical $\tilde{T}_o$). The uncertainties in the R_{mT_o} values are on the order of $\pm$ 40%, again because the T_o fluctuations are so much smaller than the m fluctuations. It should be noted that we believe that in flows with large T_o fluctuations (such as in the measurements of Laderman and Demetriades, 10) the uncertainties in the determined T_o fluctuations using our techniques will remain around $\pm$ .01 which will be a much smaller fraction of the measured values than in our flows.

As in boundary layer and wake flows (2, 10, 18) we expect to find some variation in the local mean stagnation temperature on the edge of the jet. As expected, it is in this region that we measure our highest

$\tilde{T}_o$. On the centerline of the jet, where the mean T_o distribution is flat we expect negligible T_o fluctuations, and our results predict this within the uncertainty of the measurements.

Finally the Kovasznay mode diagrams indicate that the R_{mTo} correlation coefficient is always strongly positive. This is consistent with both entropy and vorticity modes of turbulence which we would expect to be present in the flow (8).

If the assumption of negligible pressure fluctuations is made then the velocity, temperature and density fluctuations can be calculated from Equations (3.5) and (3.6). For the data presented to this point, and listed in Table II, the velocity, temperature and density fluctuation data are presented in Table III. The high level of both velocity and temperature fluctuations indicates that the vorticity and entropy modes of turbulence are approximately equally dominant.

TABLE III

ESTIMATED VELOCITY FLUCTUATIONS, TEMPERATURE FLUCTUATIONS, AND THEIR CORRELATION COEFFICIENTS IN THE M_j = 2.4 JET WITH NEGLIGIBLE PRESSURE FLUCTUATIONS

Probe Position	Figure	$\tilde{u}^+$	$\tilde{T}^+$	R_{uT}
X/D = 9, SL	17	0.149	0.106	-0.959
X/D = 5, SL†	18	0.076	0.112	-1.005
X/D = 9, CL†	19	0.055	0.116	-1.000
X/D = 5, SL; R_e = 72,900	21	0.129	0.167	-0.998

* R_{uT} cannot be less than -1.
+ Uncertainty estimates on both u and T are $\pm$ 0.02.
† The values obtained are determined from averaging all the CTA data.

This same result can be obtained by plotting Morkovin mode diagrams (14) for the experimental data presented here. Figure 22 (See Appendix C) shows an example Morkovin mode diagram; this one corresponded to a probe position of X/D = 5 on the edge of the jet. Following the procedure outlined by Morkovin (14) the velocity fluctuation, temperature fluctuation, and their correlation coefficient corresponding to this flow are $\tilde{u} = 0.0814$, $\tilde{T} = 0.1133$, and $R_{uT} = -0.9987$. These are within the experimental uncertainty of the estimates obtained from the Kovasznay mode diagram (listed in Table III).

All the mode diagrams to this point represent measurements made in the Mach number 2.4 jet. In addition several measurements were made in the Mach number 1.5 jet. Two representative mode diagrams are shown in Figures 23 and 24 (see Appendix C). The probe positions corresponding to this data are X/D = 5 on the jet edge and X/D = 9 on the centerline. For this data the agreement between the CTA data and the CCA data is not as good as in the $M_j = 2.4$ data. We have attributed the discrepency to the fact that the local mean Mach numbers for the flowfield positions are so low (M local $\simeq$ 1.36 and 1.30 for X/D = 5 and X/D = 9, respectively) that the Mach number independence assumed in the data reduction is somewhat in error. In addition, the difficulty in accurately positioning the probe has some effect on the X/D = 5 data (as it did in the $M_j = 2.4$ jet).

Because of its low Mach number, the $M_j = 1.5$ jet is not a very suitable test flow for the present experimental analysis. This is why we have concentrated on the $M_j = 2.4$ measurements. However, it should be pointed out that mass velocity fluctuation $\tilde{m}$ estimates from both CTA and CCA data in the $M_j = 1.5$ jet are in close agreement for a given probe position.

CHAPTER V

CONCLUSIONS

The experimental examples shown in Chapter IV have demonstrated that the conduction end-losses can be very important in the hot-wire measurements and results obtained from the technique without end-loss corrections can have significant differences from those obtained using the present technique. The agreement between results obtained from measurements with different hot-wire probes and different anemometers indicate that the present technique is reliable.

We have the confidence that the present technique is reliable for turbulence measurements in supersonic flows if adequate care is taken with the calibration facilities and anemometers used.

BIBLIOGRAPHY

(1) Behrens, W. "Flow Field and Stability of the Far Wake Behind Cylinders at Hypersonic Speeds." (Ph.D. thesis, California Institute of Technology, May, 1966.)

(2) Demetriades, A. "Turbulence Measurements in an Axisymmetric Compressible Wake." The Physics of Fluids, Vol. II, No. 9 (Sept., 1968), pp. 1841-1852.

(3) Demin, V. S., and N. A. Zheltukhin. "Interpretation of Hot-Wire Anemometer Readings in a Flow with Velocity, Pressure and Temperature Fluctuations." Fluid Mechanics - Soviet Research, Vol. 2, No. 3 (May-June, 1973), pp. 64-75.

(4) Dewey, C. F., Jr., Hot-Wire Measurements in Low Reynolds Number Hypersonic Flows. Hypersonic Research Project, Memorandum No. 63. Pasadena, California: Guggenheim Aero. Lab., California Institute of Technology, Sept., 1961.

(5) Kistler, A. L. "Fluctuation Measurements in a Supersonic Turbulent Boundary Layer." The Physics of Fluids, Vol. 2, No. 3 (May-June, 1959), pp. 290-296.

(6) Kovasznay, L. S. G. Calibration and Measurement in Turbulence Research by the Hot-Wire Method. NACA TM No. 1130. Washington, D. C.: National Advisory Committee for Aeronautics, June, 1947.

(7) Kovasznay, L. S. G. "The Hot-Wire Anemometer in Supersonic Flow." Journal of the Aero. Science, Vol. 17, No. 9 (Sept., 1950), pp. 565-572.

(8) Kovasznay, L. S. G. "Turbulence in Supersonic Flow." Journal of the Aero. Science, Vol. 20, No. 10 (Oct., 1953), pp. 657-674.

(9) Kovasznay, L. S. G. "Interaction of a Shock Wave and Turbulence." Heat Transfer and Fluid Mechanics Institute, University of California, Los Angeles, 1955.

(10) Laderman, A. J. and A. Demetriades. "Mean and Fluctuating Flow Measurements in the Hypersonic Boundary Layer Over a Cooled Wall." Journal of Fluid Mechanics, Vol. 63, No. 1 (March, 1974), pp. 121-144.

(11) Laufer, J. "Aerodynamic Noise in Supersonic Wind Tunnels." Journal of the Aero. Science, Vol. 28 (Sept., 1961), pp. 685-692.

(12) Lord, R. G. "Hot-Wire Probe End-Loss Correction in Low Density Flows." Journal of Physics E; Scientific Instruments, Vol. 7 (Jan., 1974), pp. 56-60.

(13) McLaughlin, D. K., G. L. Morrison and T. R. Troutt. "Experiments on the Instability Waves in a Supersonic Jet and Their Acoustic Radiation." Journal of Fluid Mechanics, Vol. 69, Part 1, (April, 1975), pp. 73-95.

(14) Morkovin, M. V. Fluctuations and Hot-Wire Anemometry in Compressible Fluids. AGARDograph No. 24, Paris: NATO, November, 1956.

(15) Morkovin, M. V. and R. E. Phinney. Extended Applications of Hot-Wire Anemometry to High-Speed Turbulent Boundary Layers. AFOSR TN-58-469. Baltimore, Maryland: Dept. of Aeronautics, The Johns Hopkins University, June, 1958.

(16) Morkovin, M. V. "Signal Interpretation in High-Speed Anemometry." Advances in Hot-Wire Anemometry. Proc. Intern. Symposium on Hot-Wire Anemometry, University of Maryland, March 20-21, 1967, pp. 38-51.

(17) Owen, F. K., C. C. Horstman and M. I. Kussoy. "Mean and Fluctuating Flow Measurements of a Fully-Developed, Non-Adiabatic, Hypersonic Boundary Layer." Journal of Fluid Mechanics, Vol. 70, Pt. 2 (Aug., 1975), pp. 393-413.

(18) Rose, W. C. The Behavior of a Compressible Turbulent Boundary Layer in a Shock-Wire-Induced Adverse Pressure Gradient. NASA TN D-7092. Moffett Field, Calif.: Ames Research Center, March, 1973.

(19) Rose, W. C. Turbulence Measurements in a Compressible Boundary Layer." AIAA Journal, Vol. 12, No. 8 (Aug., 1974), pp. 1060-1064.

(20) Vrebalovich, T. Application of Hot-Wire Technique in Unsteady Compressible Flows. TR No. 32-229. Pasadena, Calif.: Jet Propulsion Lab. California Institute of Technology, May, 1962.

(21) Vrebalovich, T. "Heat Loss and Recovery Temperature of Fine Wires in Transonic Transition Flow." Rarefield Gas Dynamics. Vol. II. New York: Academic Press, 1967, pp. 1205-1219.

(22) Wagner, R. D. Mean Flow and Turbulence Measurements in a Mach 5 Free Shear Layer. NASA TN D-7366. Washington, D. C.: National Aeronautics and Space Administration, December, 1973.

APPENDIX A

KOVASZNAY MODE DIAGRAM CURVE FITTING

APPENDIX A

KOVASZNAY MODE DIAGRAM CURVE FITTING

The mass velocity fluctuation $\tilde{m}$, the stagnation temperature fluctuation $\tilde{T}_o$, and their correlation coefficient R_{mTo} of the presented CTA data were determined from second order polynomial regression curve fits of the data of $(\tilde{e}/A_T)^2$ versus A_m/A_T into the form of Equation (2.29) (see Figure 25, Appendix C). The resultant curve shown in Kovasznay coordinates ($\tilde{e}/A_T$ versus A_m/A_T) becomes a hyperbola (see Figure 26, Appendix C). The fluctuation properties obtained from this procedure should be very reasonable and straight-forward. However, difficulties can arise since physically unreasonable situations can result from inaccuracies of individual data points. Minor adjustments have to be imposed in order to obtain physically reasonable results.

As shown in Figure 25 (Appendix C), the second order curve from the regression fit of the data of $(\tilde{e}/A_T)^2$ versus A_m/A_T can only lie in the first quadrant since both the ordinate and abscissa are positive definite quantities. However, mathematically, the fitted curve can exist in any quadrant as long as it meets the requirement of the least square of errors, even though all the data points appear in the first quadrant only. Figure 27 (Appendix C) shows a physically unreasonable regression fit for the CTA data where the probe is positioned at X/D = 5 on shear annulus of the M_j = 2.4 jet.

The fitted curve of Figure 27 (Appendix C) passes into the fourth

quadrant indicating negative values of $(\tilde{e}/A_T)^2$ which are physically unreasonable. The correlation coefficient R_{mTo} for this particular curve fit is 1.028 which is also physically impossible since by definition R_{mTo} must fall between -1 and +1. In addition, a portion of the mode diagram in Kovasznay coordinates actually becomes imaginary in a portion of the plot (see Figure 28, Appendix C). In this situation we correct the difficulty by constraining R_{mTo} to be 1.00 which produces a new curve shown in Figure 18 (Appendix C).

This regression analysis can also run into difficulties when the total temperature fluctuations $\tilde{T}_o$ of the flow are so small that the experimental inaccuracies in low overheat data points render the intercept of the regression curve to be negative and hence, unreasonable. (It is physically impossible to have negative values of $\tilde{T}_o^2$.) Figure 29 (Appendix C) shows the regression curve with a negative intercept of $(\tilde{e}/A_T)^2$ for the CTA data at X/D = 9, centerline position of the M_j = 2.4 jet. The corresponding curve in Kovasznay mode diagram (Figure 30, Appendix C) becomes imaginary near the origin and it yields a $\tilde{T}_o^2$ value to be -0.0000149. This unreasonable result was corrected by constraining the total temperature fluctuation $\tilde{T}_o$ to be zero and hence, the curve in the Kovasznay mode diagram becomes a straight line passing through the origin (see Figure 19, Appendix C).

Since the shape of the regression curve is very sensitive to the experimental errors of data points, especially of low over heat ratio data, it is very important to reduce the experimental inaccuracies as much as possible during the experiment. If care is taken with the experiments and if reasonable constraints are placed on the curve fits, output data which is in good agreement with physical intuition is possible.

APPENDIX B

SUMMARY OF DATA REDUCTION TECHNIQUES IN BOTH CTA AND CCA OPERATION

APPENDIX B

SUMMARY OF DATA REDUCTION TECHNIQUES IN BOTH CTA AND CCA OPERATION

Constant Temperature Operation

(1) Complete mean flow calibration producing data such as that shown in Figure 5 (Appendix C).

(2) From interpolation produce constant overheat curves such as shown in Figure 6 (Appendix C).

(3) For the point in the flowfield where modal decomposition is to be performed determine mean (ρu) from $\overline{E}$ and a_w measurements and data of Figure 6 (Appendix C).

(4) From (ρu) determined in (3) and measured T_r (and hence T_o from estimate of η) compute local Re_o on hot-wire.

(5) From determined Re_o find a better estimate of η and hence recompute T_o and Re_o.

(6) For the mean (ρu) value determine $\left.\frac{\partial \ell n \overline{E}}{\partial \ell n \overline{\rho u}}\right|_{R_w,\ T_o}$ as a function of a_w from the data of Figure 5 (Appendix C).

(7) Plot the logarithmic derivatives $\left.\frac{\partial \ell n \overline{E}}{\partial \ell n \overline{\rho u}}\right|_{R_w,\ T_o} = A_m$ as a function of overheat ratio as shown in Figure 11 (Appendix C).

(8) Determine all values of ε from Equation (2.32) using A_m data from step (7) and log derivative data knowing mean Reynolds number of the flow position.

(9) Calculate A_T from Equation (2.27) and plot as a function of wire overheat as shown in Figure 12 (Appendix C).

(10) Plot Kovasznay mode diagram from $\tilde{e}$, A_m and A_T data.

Constant Current Operation

(1) Complete mean flow calibration producing data such as that shown in Figure 7 (Appendix C).

(2) By interpolation produce curves of constant overheat ratio similar to Figure 6 (Appendix C) in CTA operation. Determine mean ρu of point in flowfield from this data.

(3) For the mean (ρu) value, hot-wire E and I, and the vacuum calibration data, calculate ε as a function of wire overheat, using Lord's procedure.

(4) From (ρu) determined in (2) and from measured T_r (and hence T_o from estimate of η) compute local Re_o on wire.

(5) From determined Re_o find a better estimate of η hence recompute T_o and Re_o.

(6) From determined ε and logarithmic derivatives of mean flow data calculate B_m and B_T for range of overheat from Equations (2.41), (2.42), and (2.43). This produces the data of Figures 11 and 12 (Appendix C).

(7) Plot Kovasznay mode diagram from $\tilde{e}$, B_m, and B_T data.

APPENDIX C

FIGURES

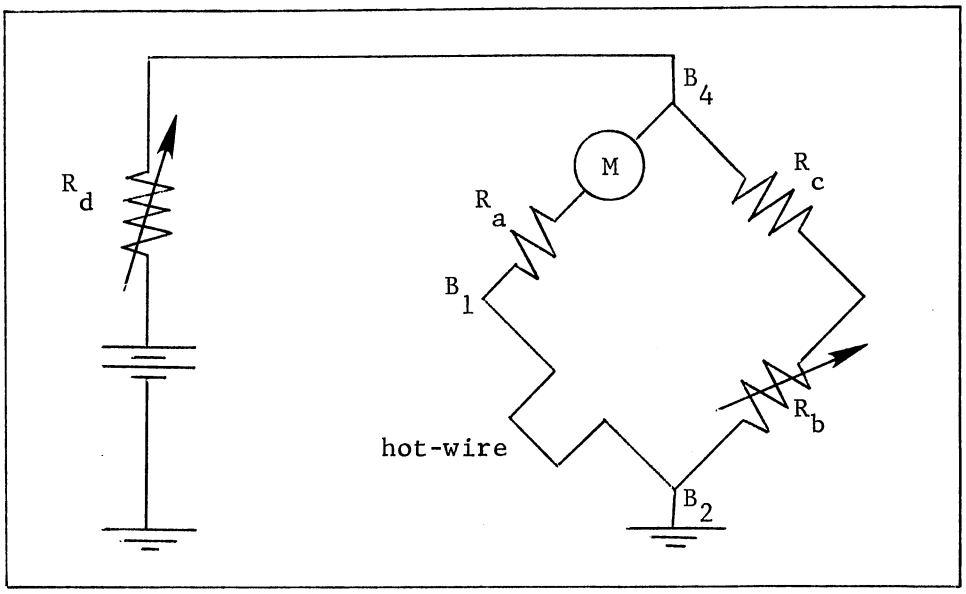

Figure 1. CCA Bridge Circuit

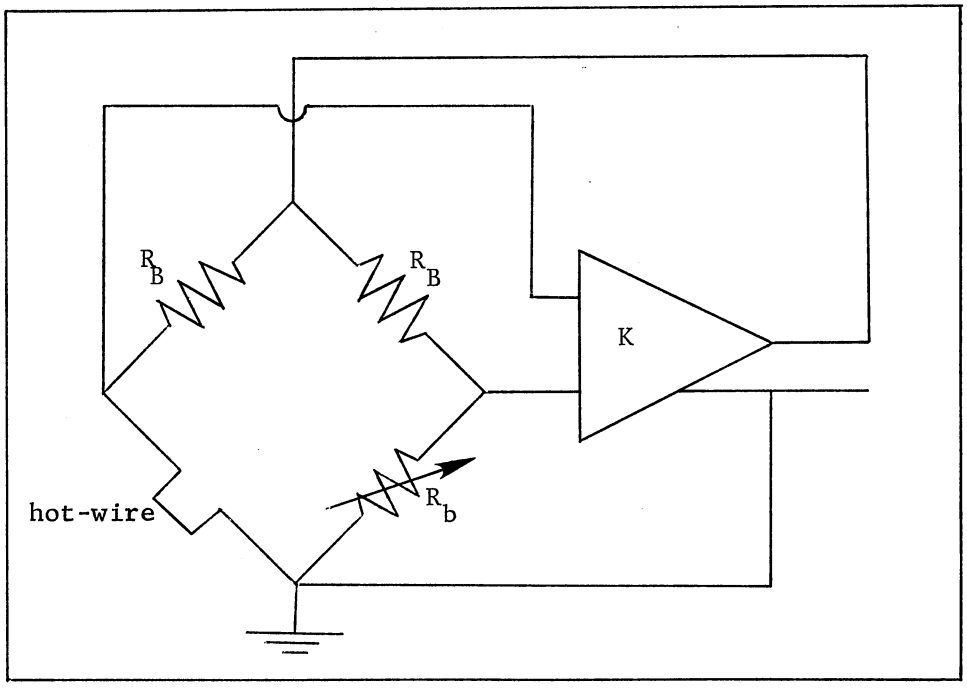

Figure 2. CTA Bridge Circuit

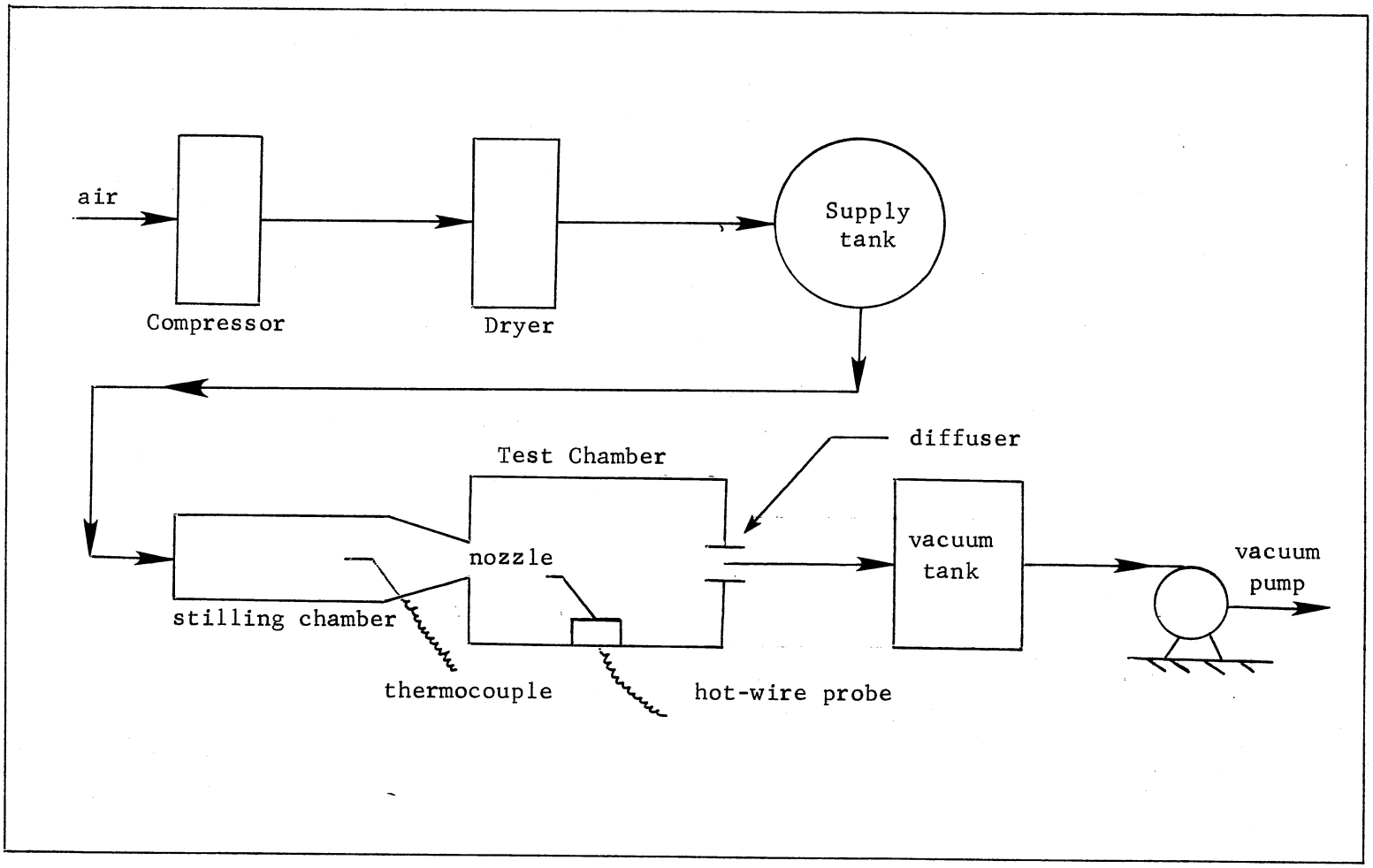

Figure 3. Experimental Facilities.

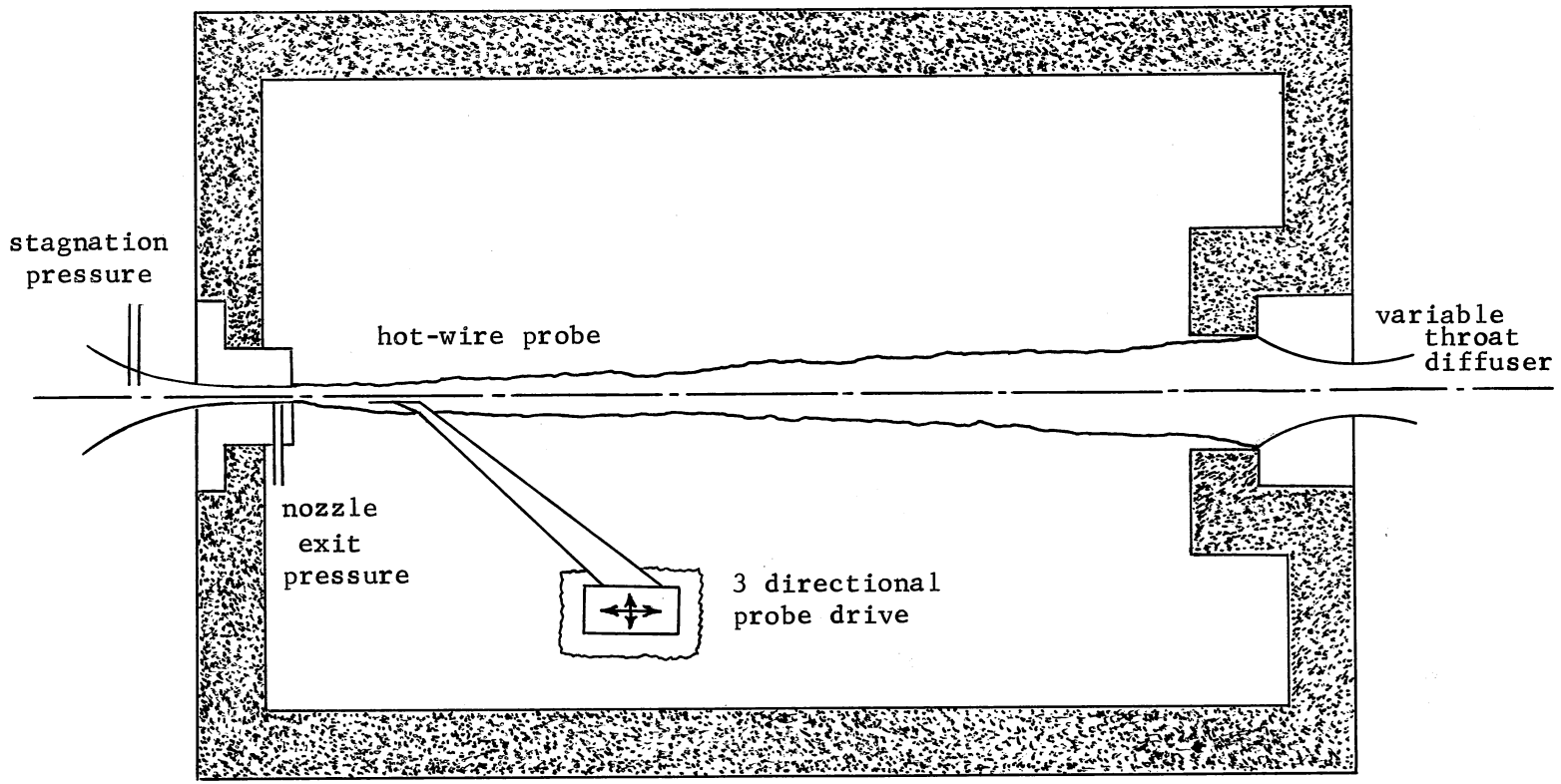

Figure 4. Schematic of Anechoic Vacuum Chamber Jet Test Facility.

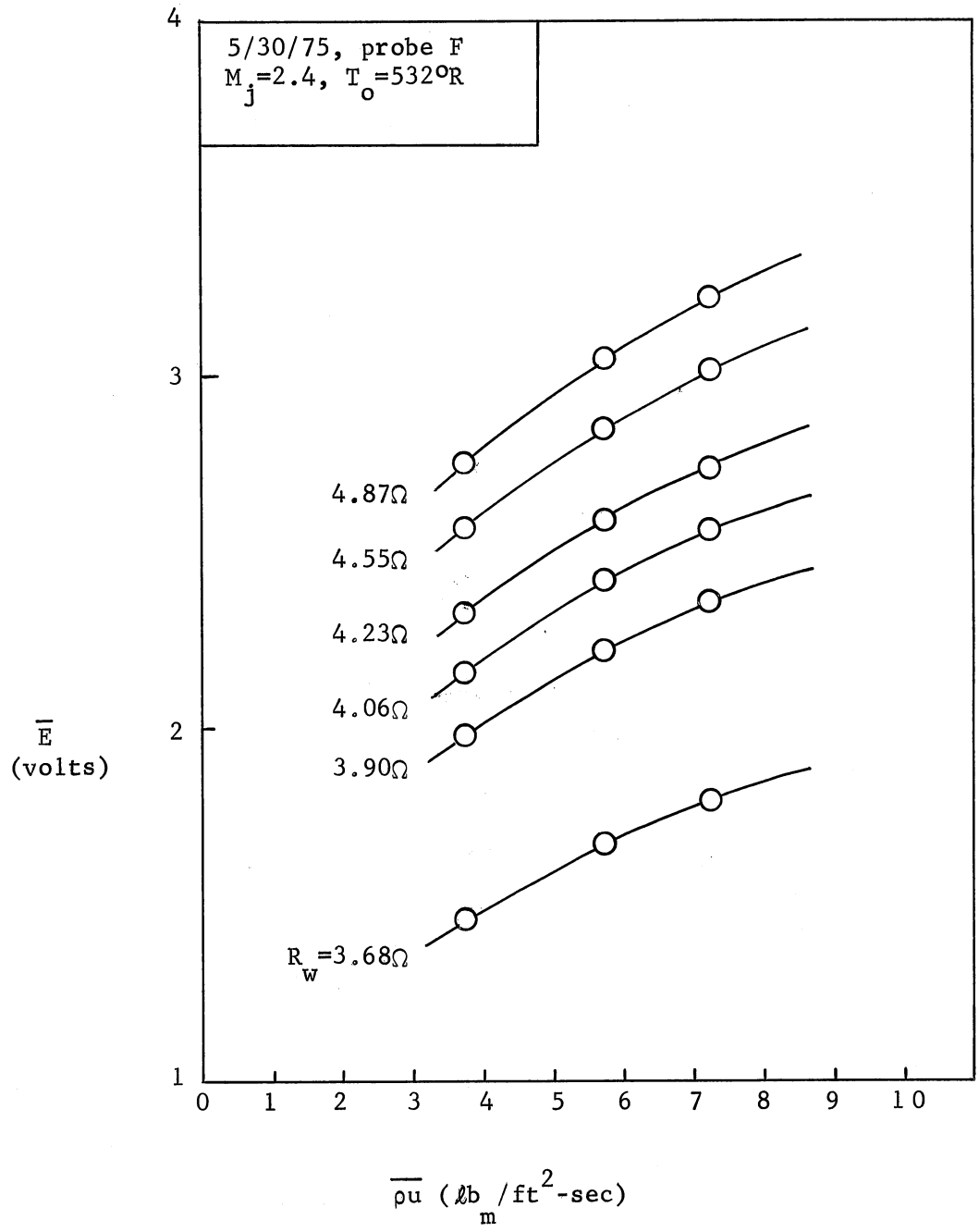

Figure 5. CTA Mean Flow Calibration (Constant) Resistance Curves).

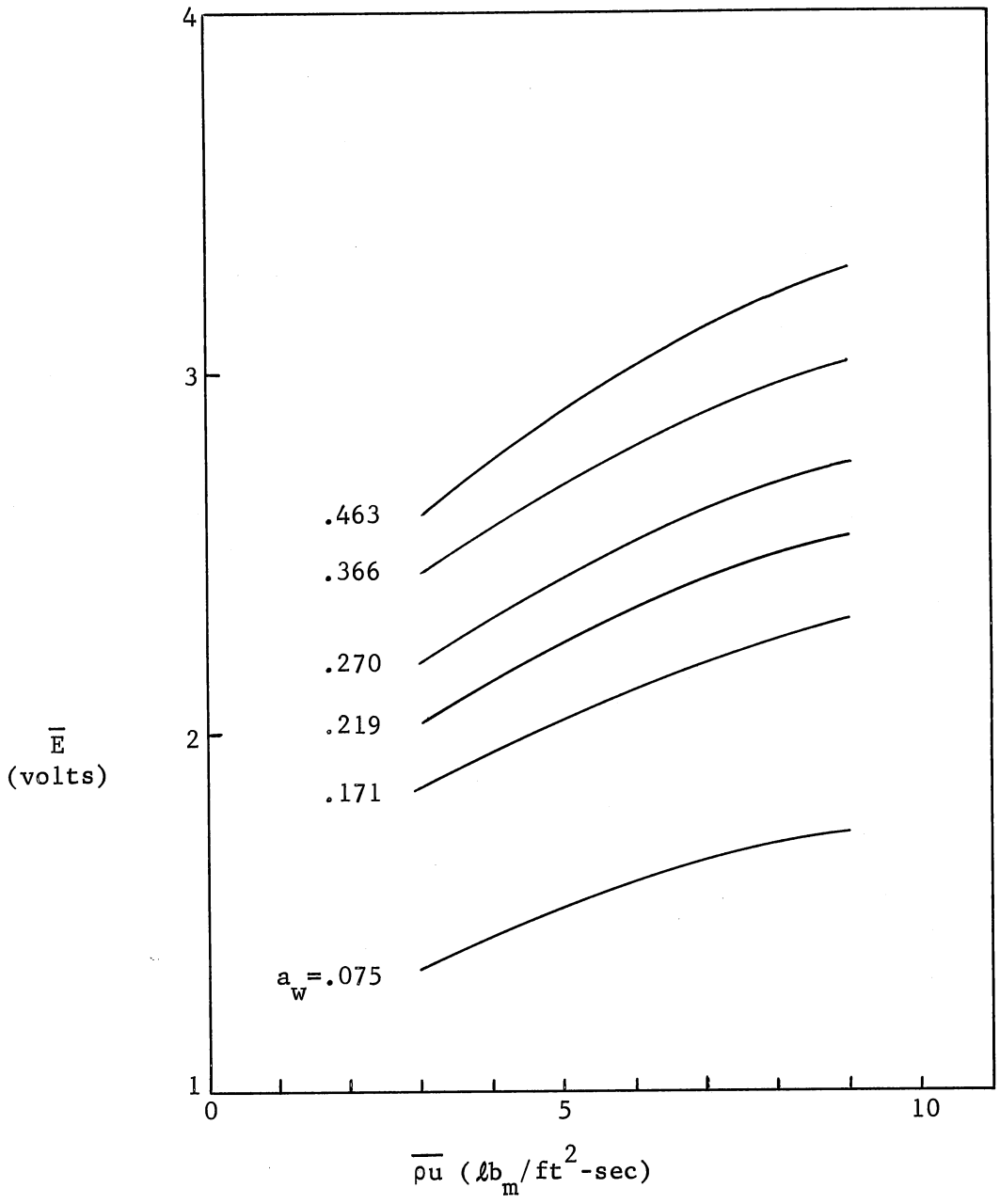

Figure 6. CTA Constant Overheat Ratio Curves Obtained by Interpolation from the Data of Figure 5.

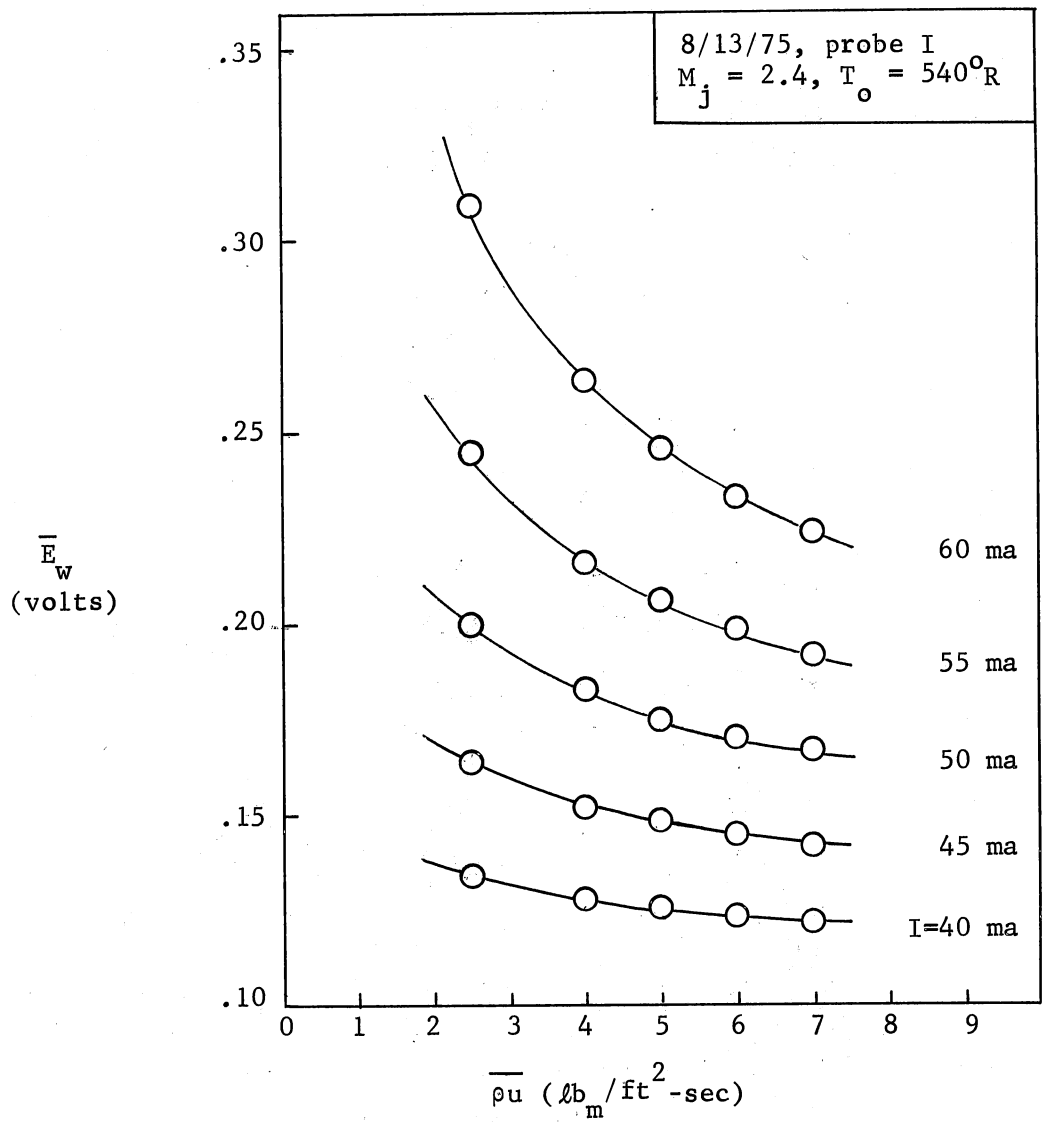

Figure 7. CCA Mean Flow Calibration of Wire Voltage with Constant Currents.

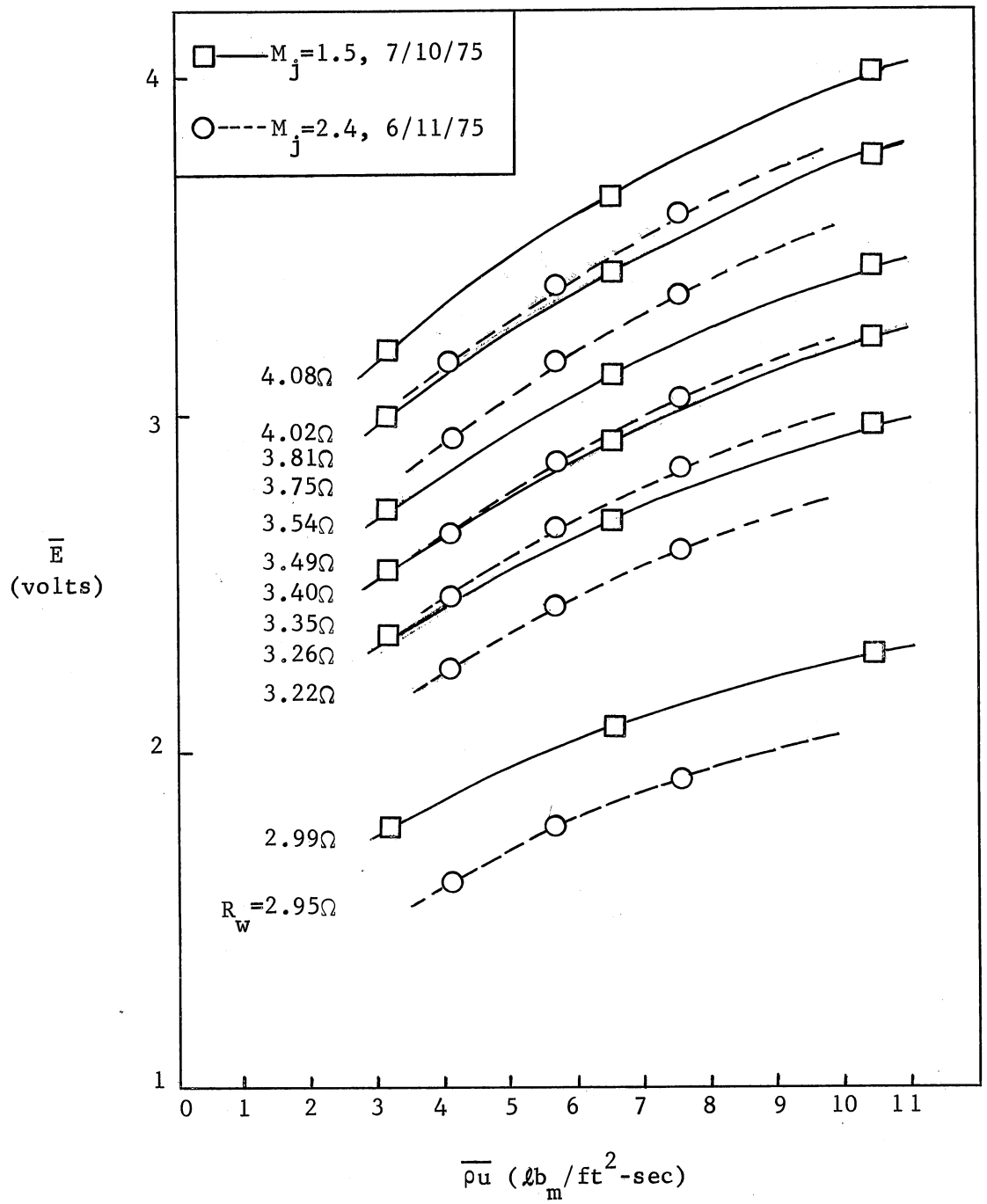

Figure 8. Comparison of CTA Mean Flow Calibrations with the Same Hot-Wire Probe at Two Different Mach Numbers.

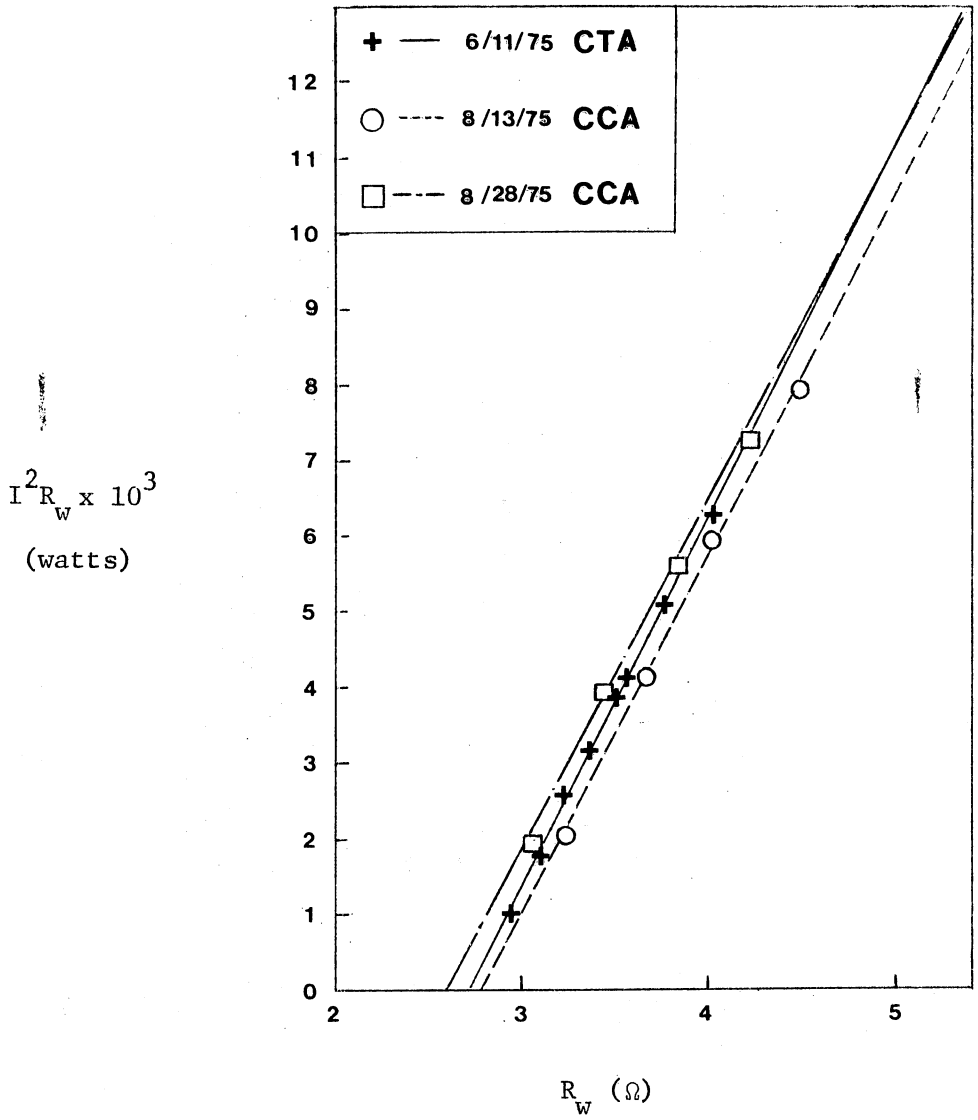

Figure 9. Comparison of Vacuum Calibrations with the Same Probe.

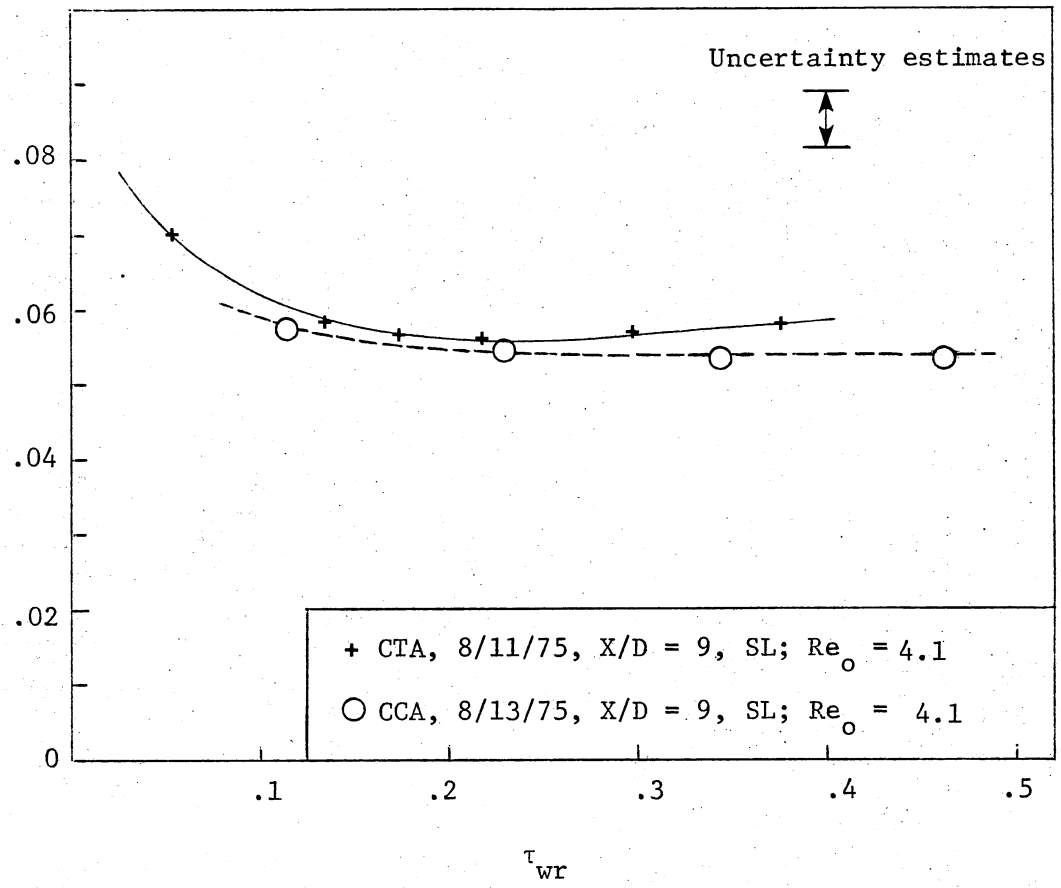

Figure 10. Variation of Conduction End-Loss Ratio with Overheat Ratio.

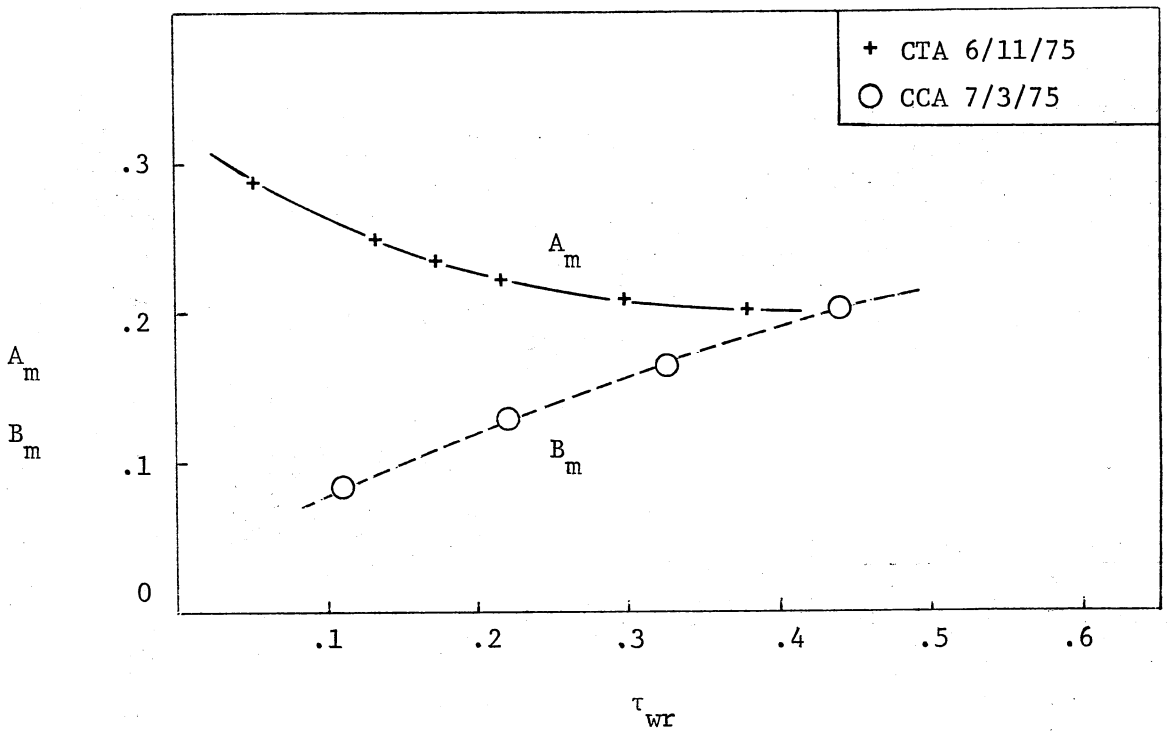

Figure 11. Mass Velocity Sensitivities as a Function of Overheat Ratio (X/D = 9, CL; M_j = 2.4).

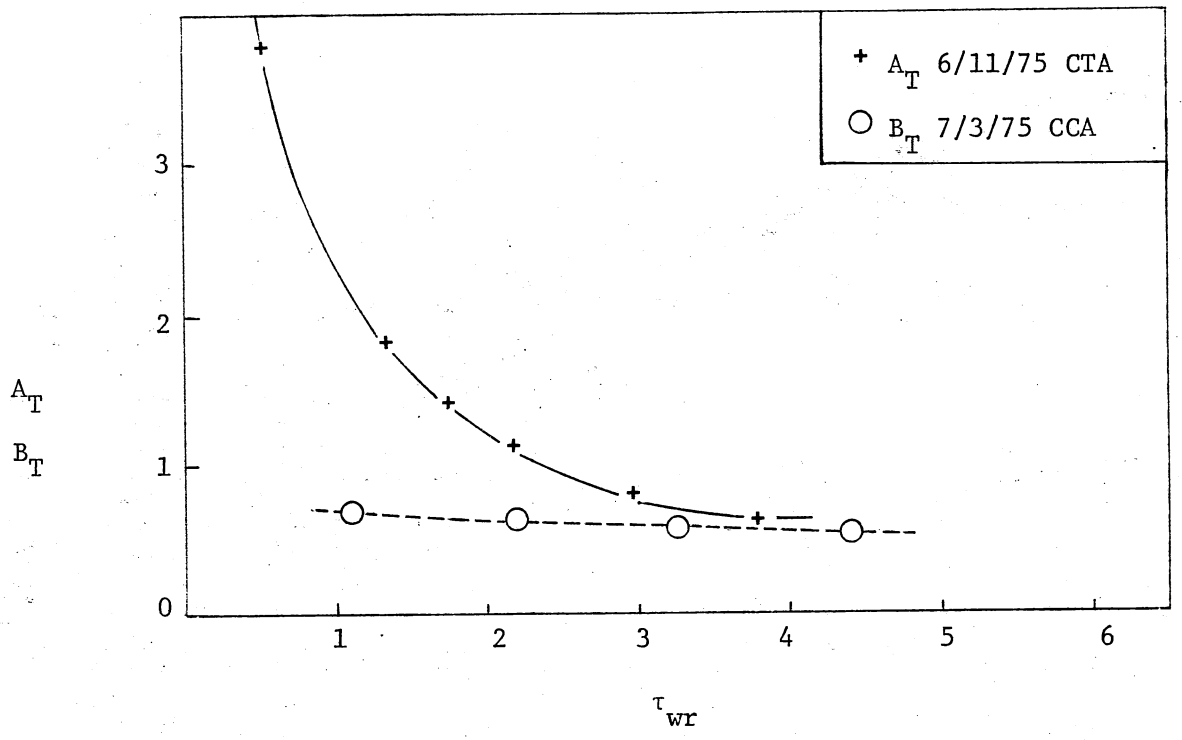

Figure 12. Stagnation Temperature Fluctuation Sensitivity as a Function of Overheat Ratio.

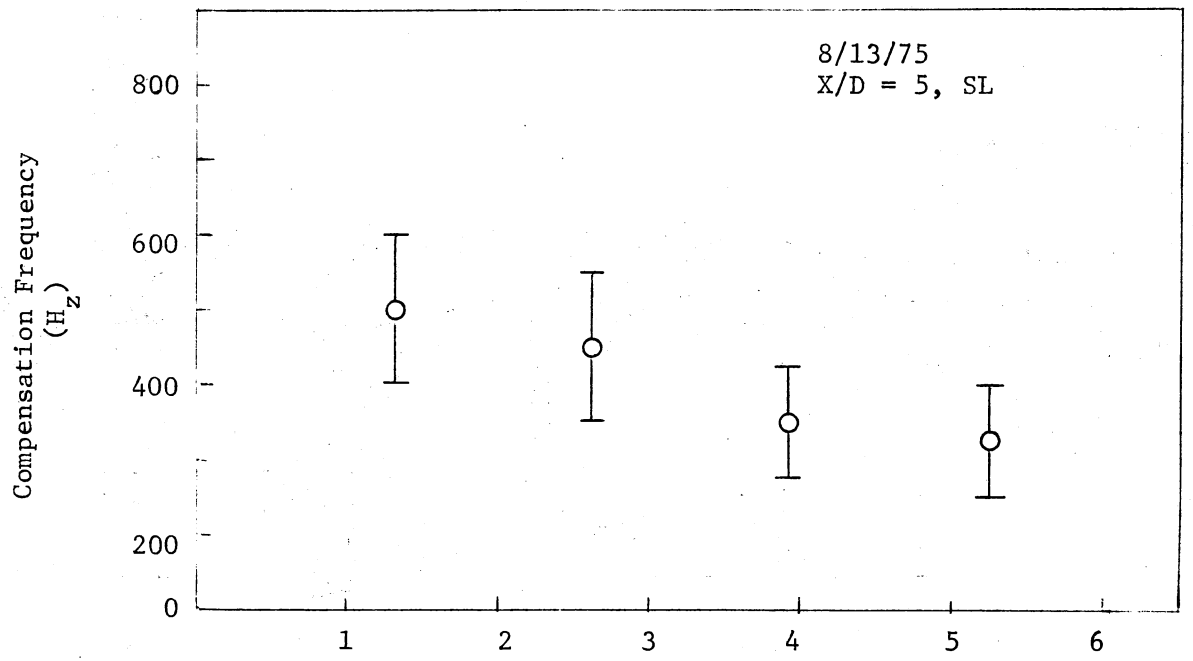

Figure 13. Estimated Compensation Frequencies with Error Bands for CCA System.

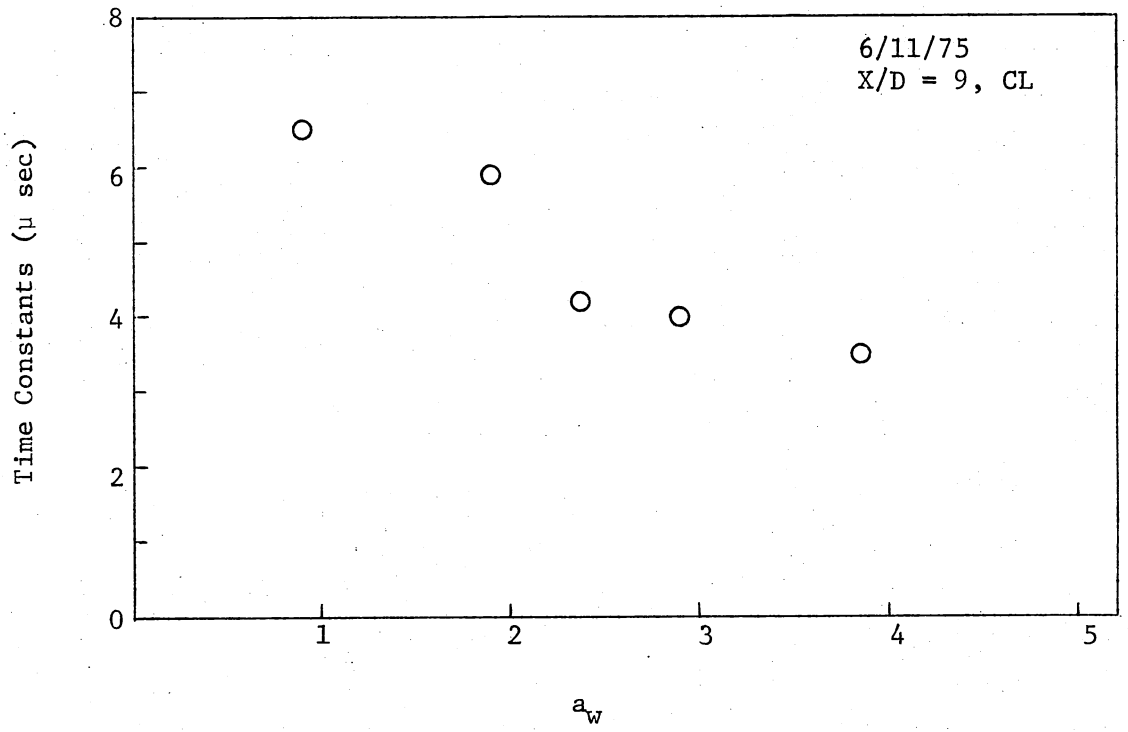

Figure 14. Variation of Time Constants with Respect to Overheat Ratios for CTA System.

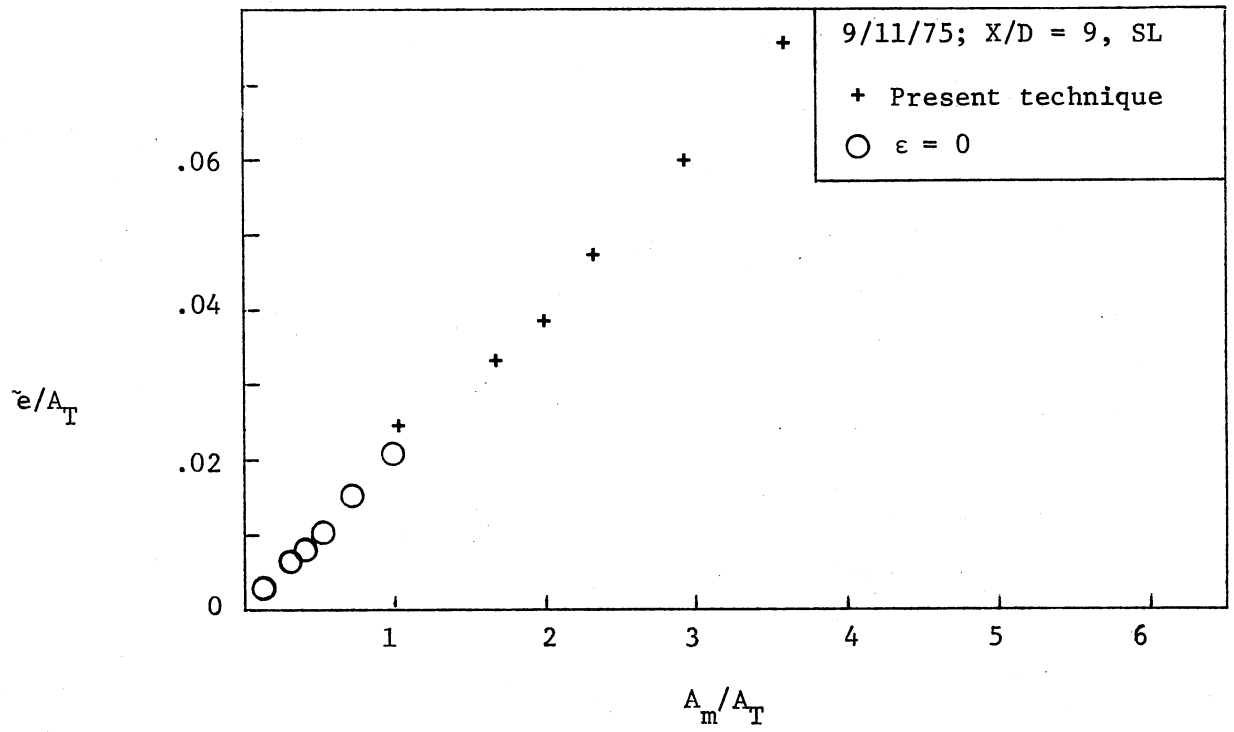

Figure 15. Comparison Between Results Obtained from Present Techniques and from the Technique with Partial End-Loss.

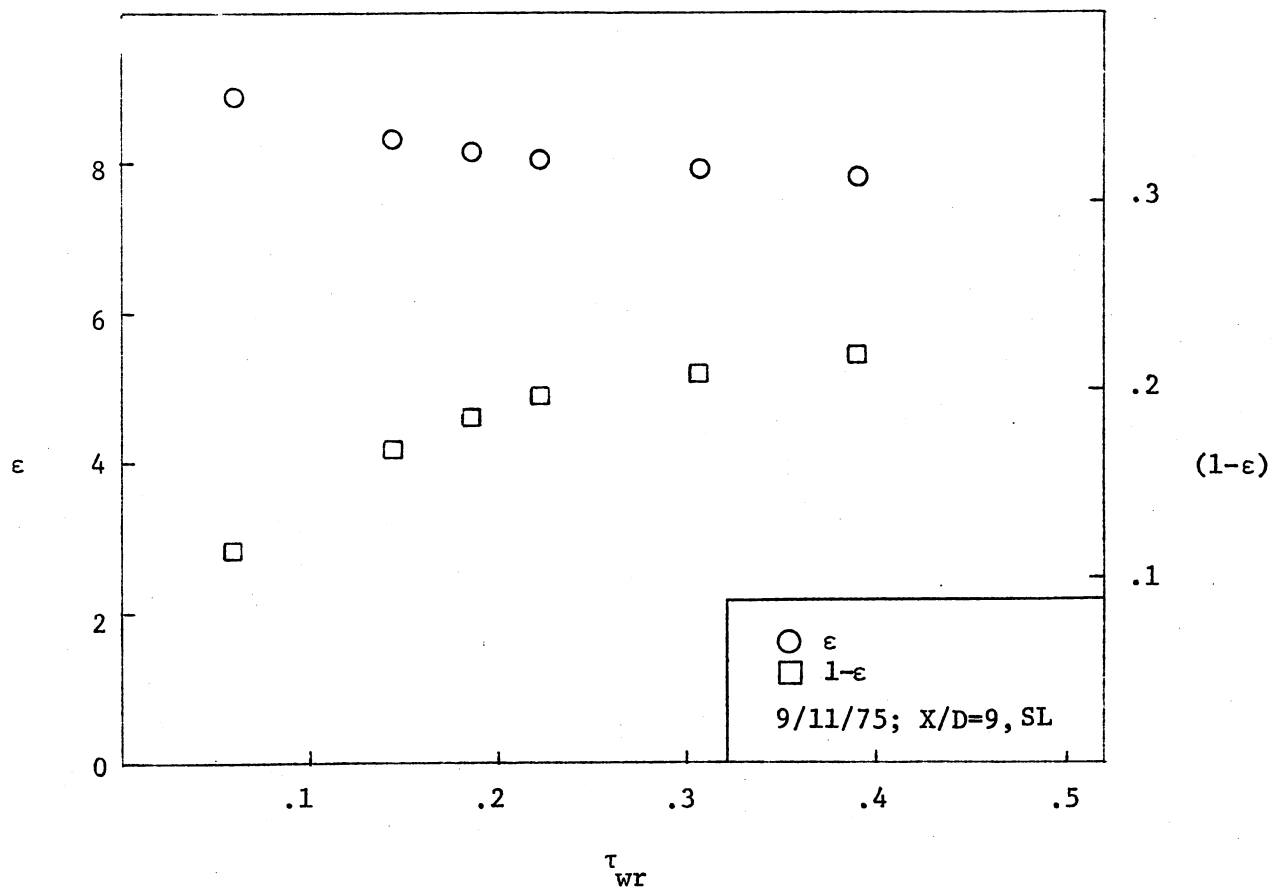

Figure 16. Conduction End-Loss Ratio as a Function of Overheat Ratio.

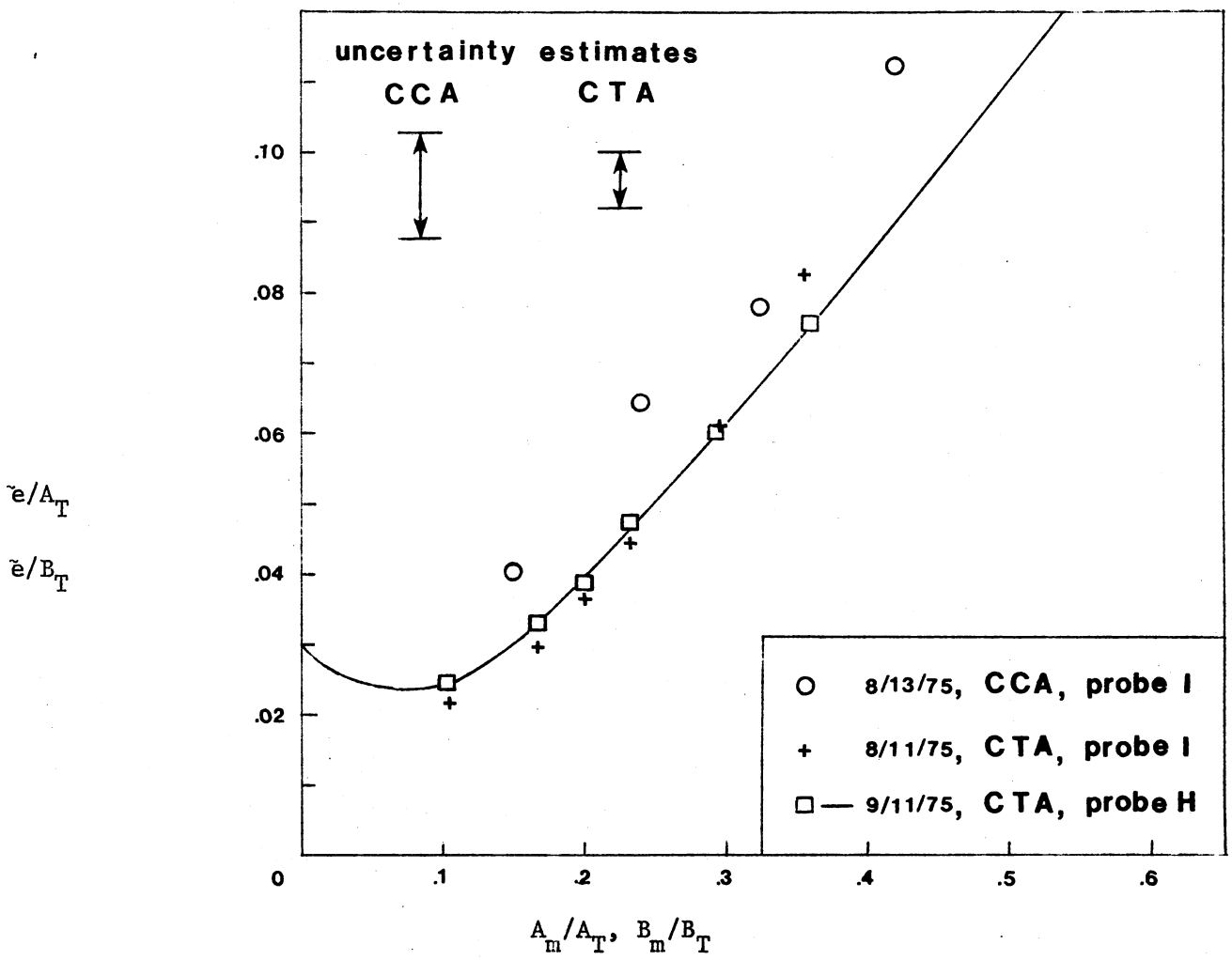

Figure 17. Comparison of Experimental Results for the Position of X/D = 9 on the Edge of the M_j = 2.4 Jet.

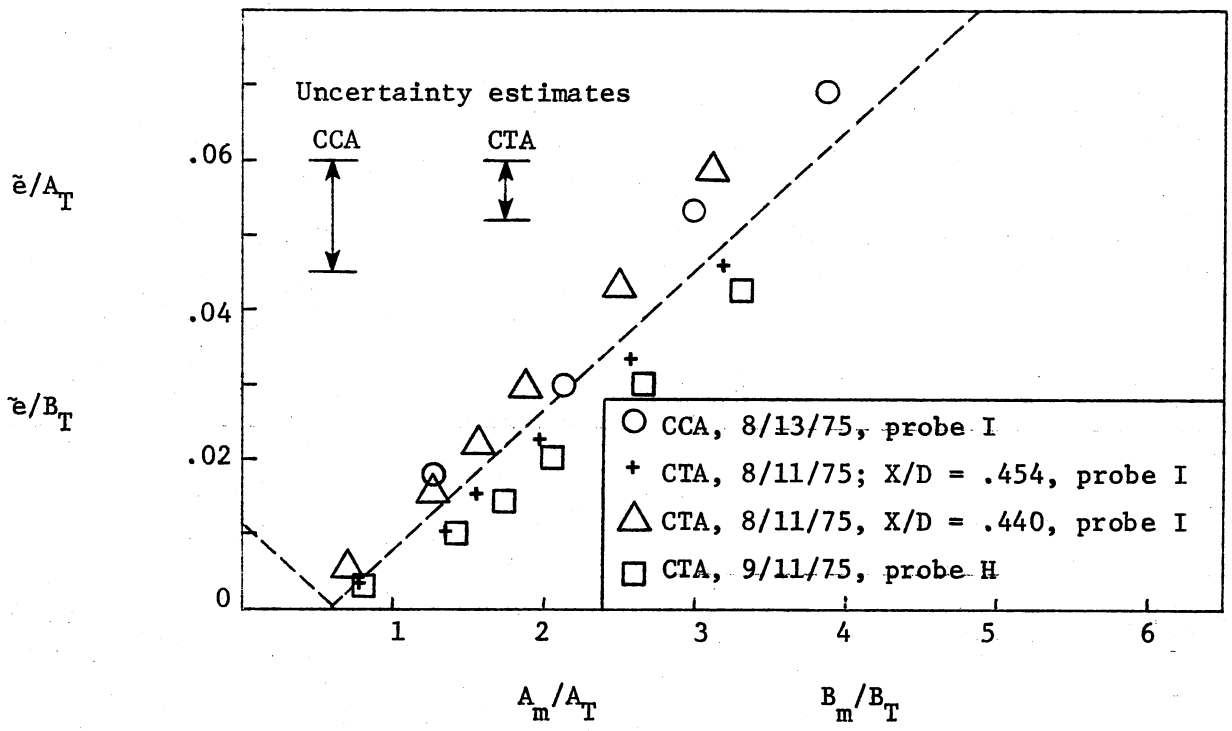

Figure 18. Comparison of Experimental Results for the Position of X/D = 5 on the Edge of the M_j = 2.4 Jet.

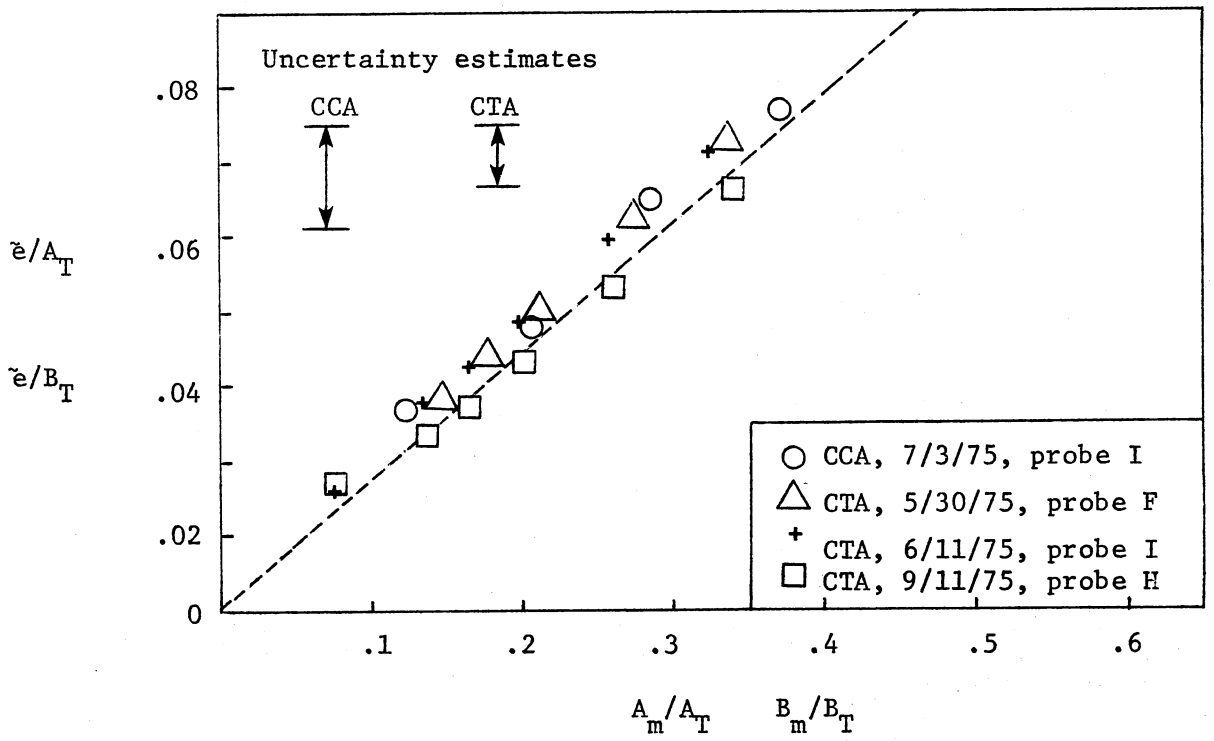

Figure 19. Comparison of Experimental Results for X/D = 9 Center Line of the M_j = 2.4 Jet.

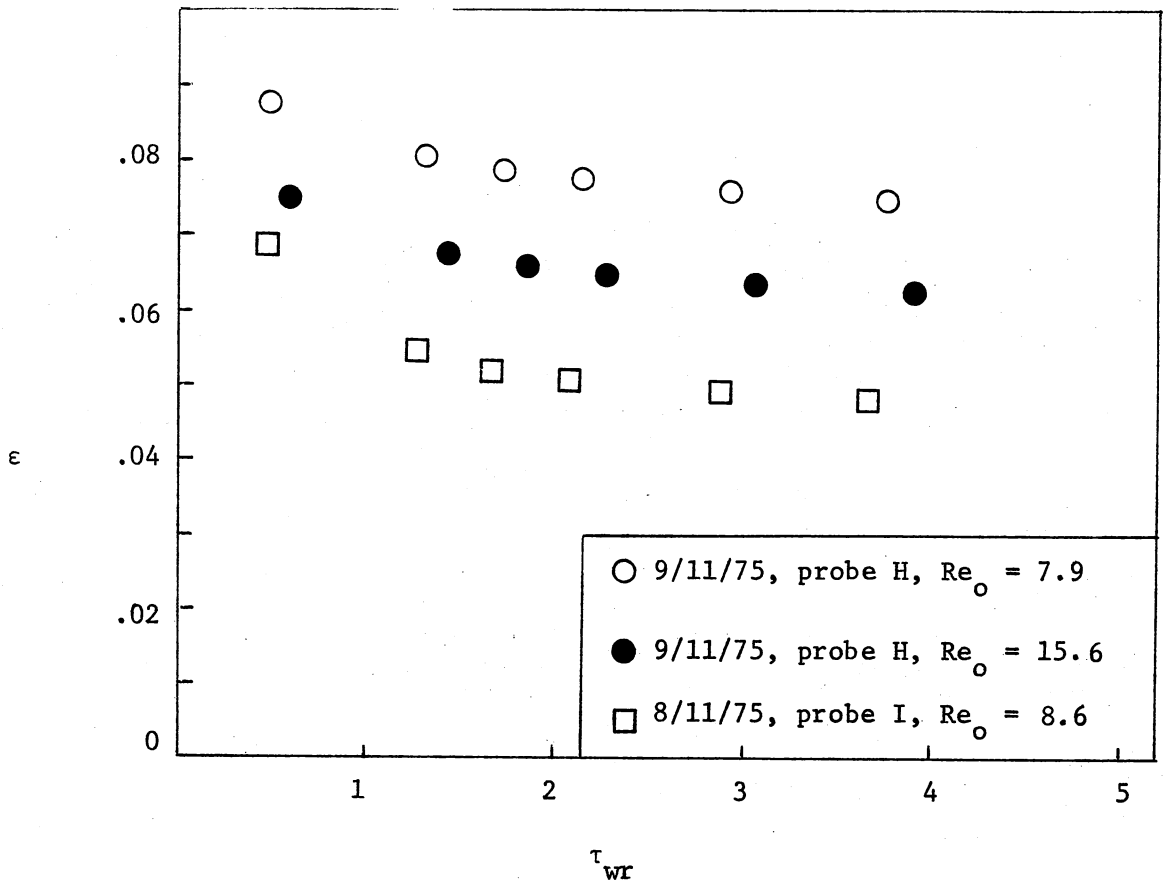

Figure 20. Conduction End-Loss Ratios as a Function of Overheat Ratio at X/D = 5, on the Edge of the M_j = 2.4 Jet.

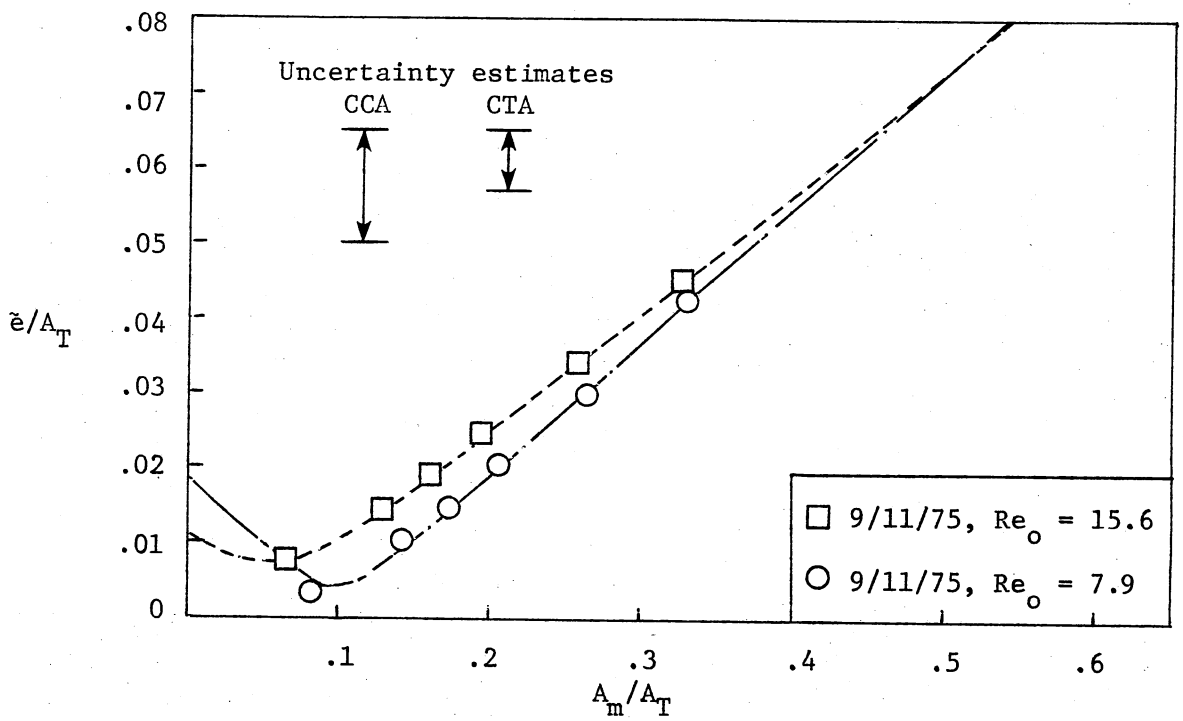

Figure 21. Comparison of Results for X/D = 5, on the Edge of the M_j = 2.4 Jet with Two Different Reynolds Numbers.

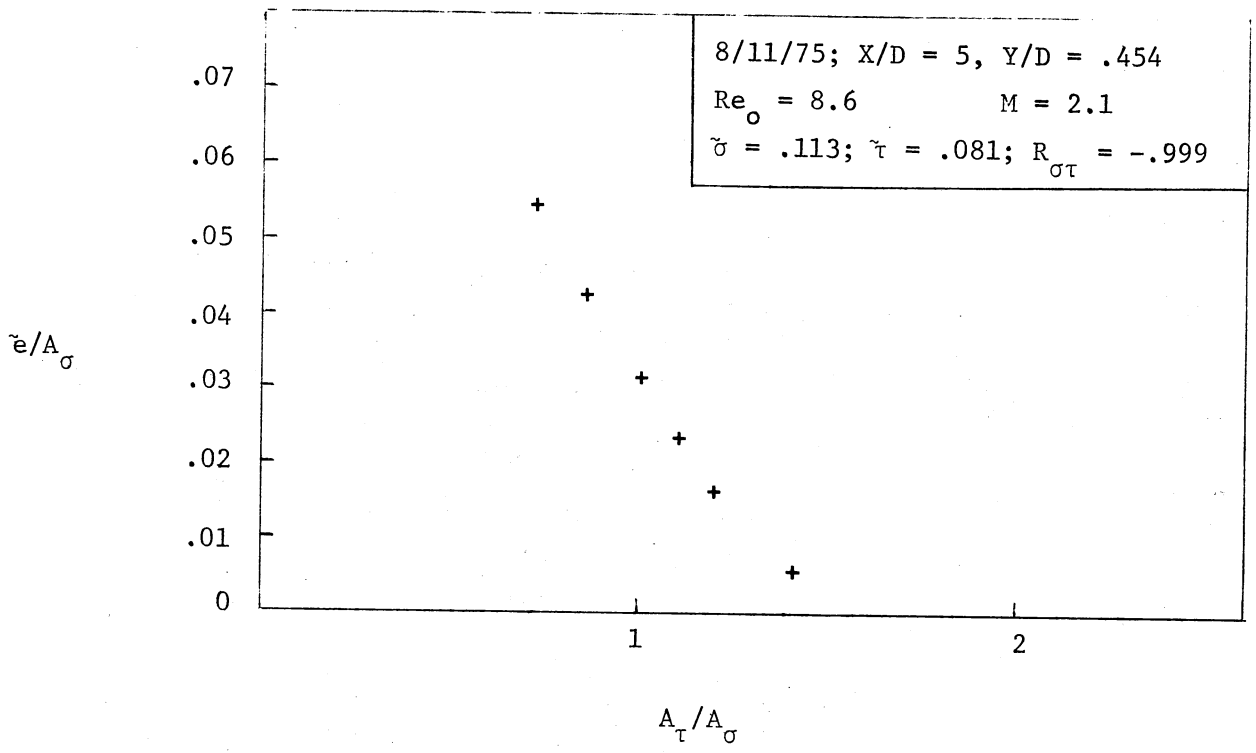

Figure 22. Morkovin Mode Diagram for X/D = 5, on the Edge of the M_j = 2.4 Jet (8/11/75, CTA Data).

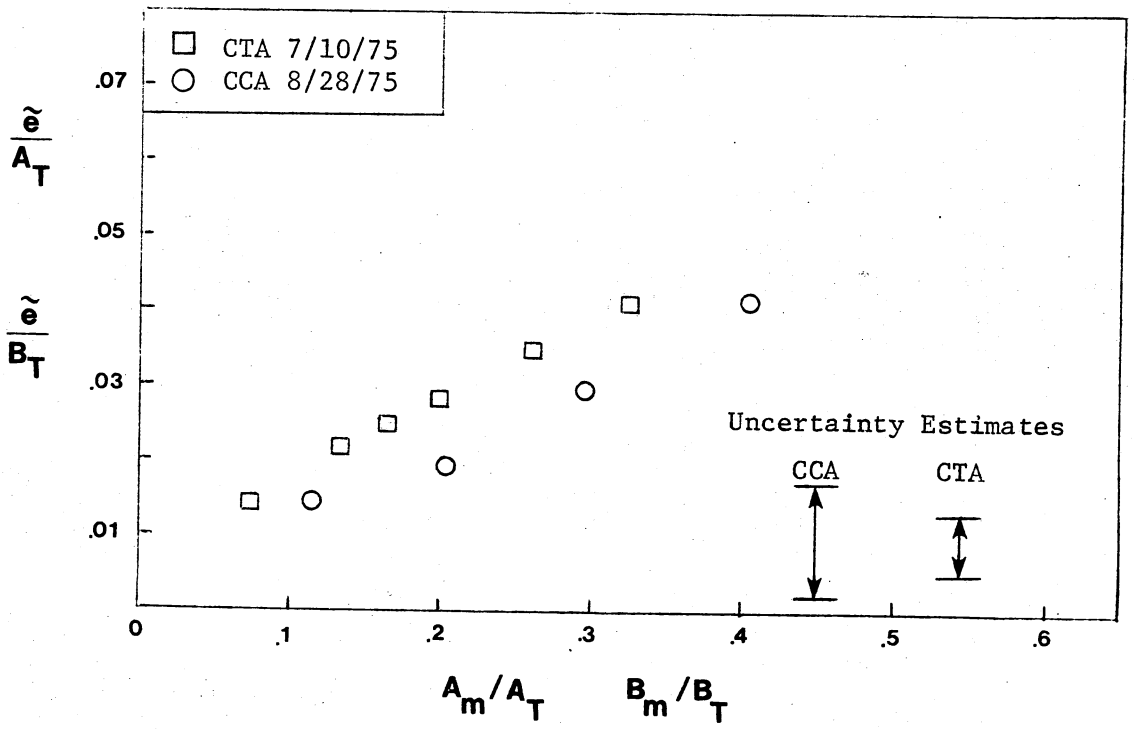

Figure 23. Comparison of Results for X/D = 5, on the Edge of the M_j = 1.5 Jet.

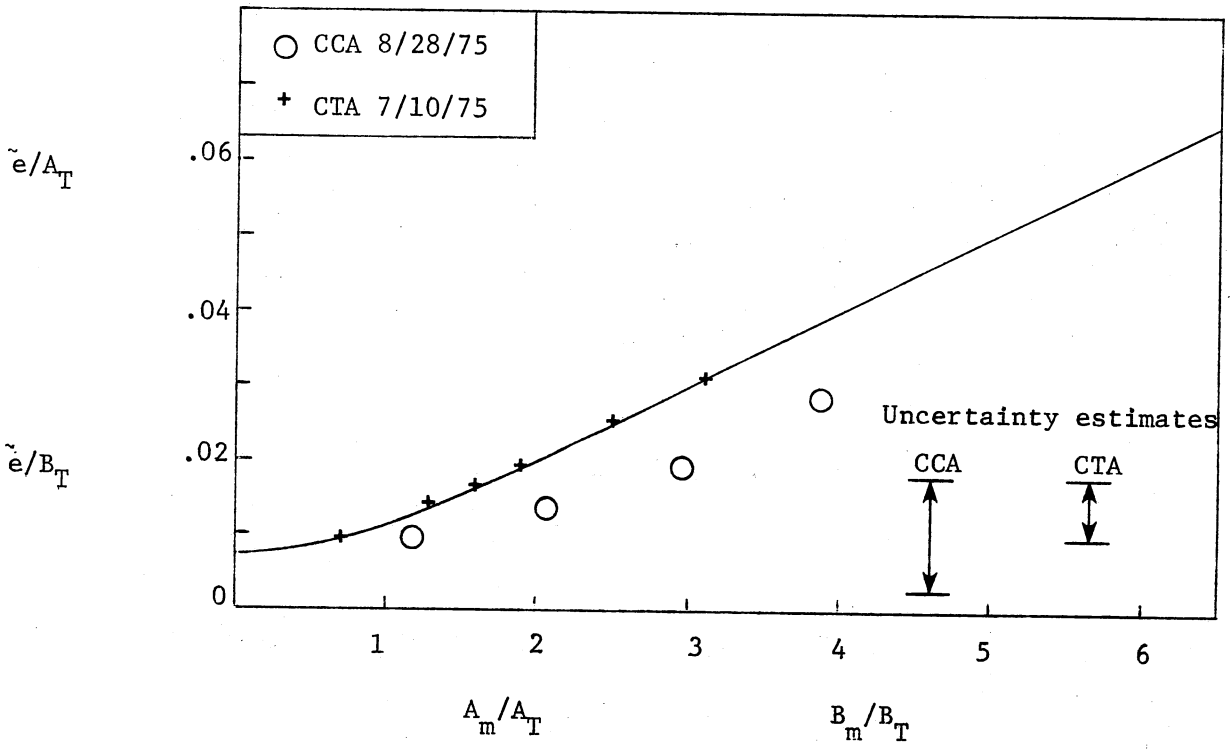

Figure 24. Comparison of Results for X/D = 9, Center Line of the M_j = 1.5 Jet.

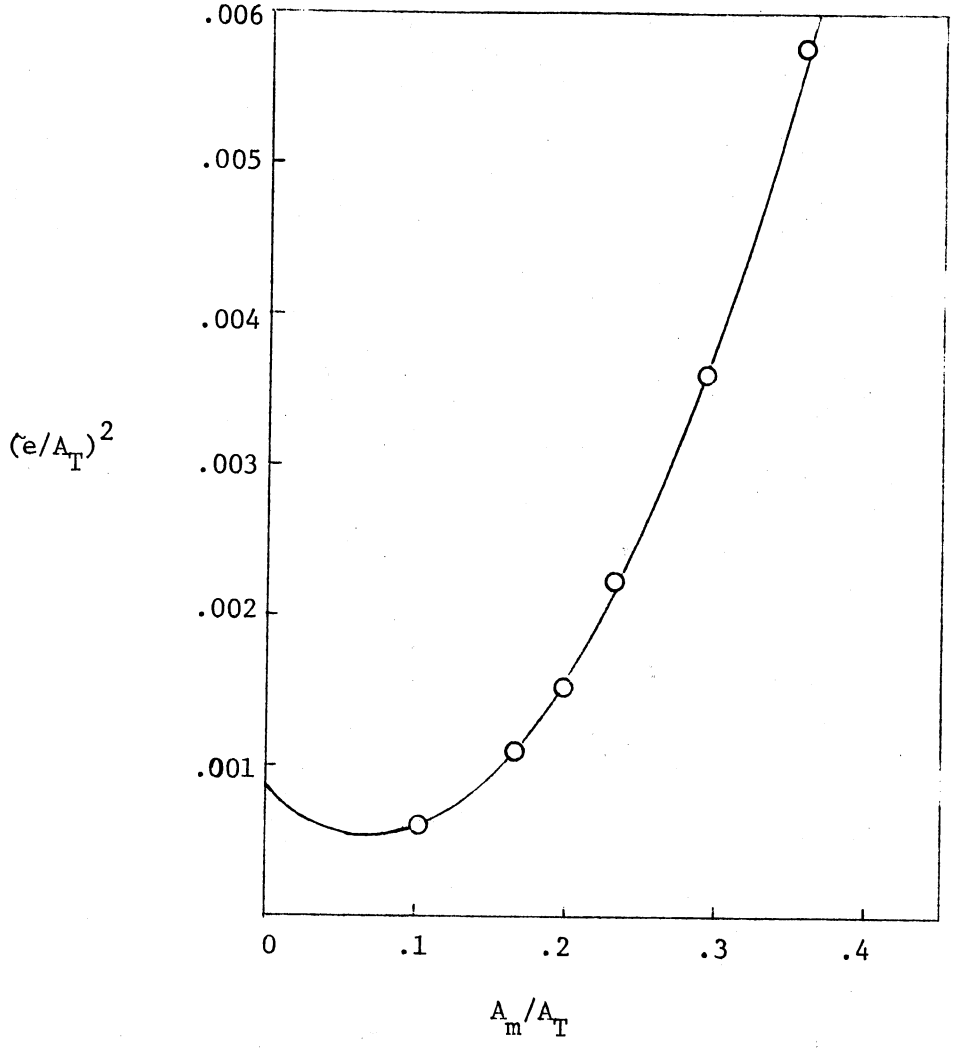

Figure 25. The Second Order Regression Curve Fit for 9/11/75 Data at X/D = 9, on the Shear Layer of the M_j = 2.4 Jet.

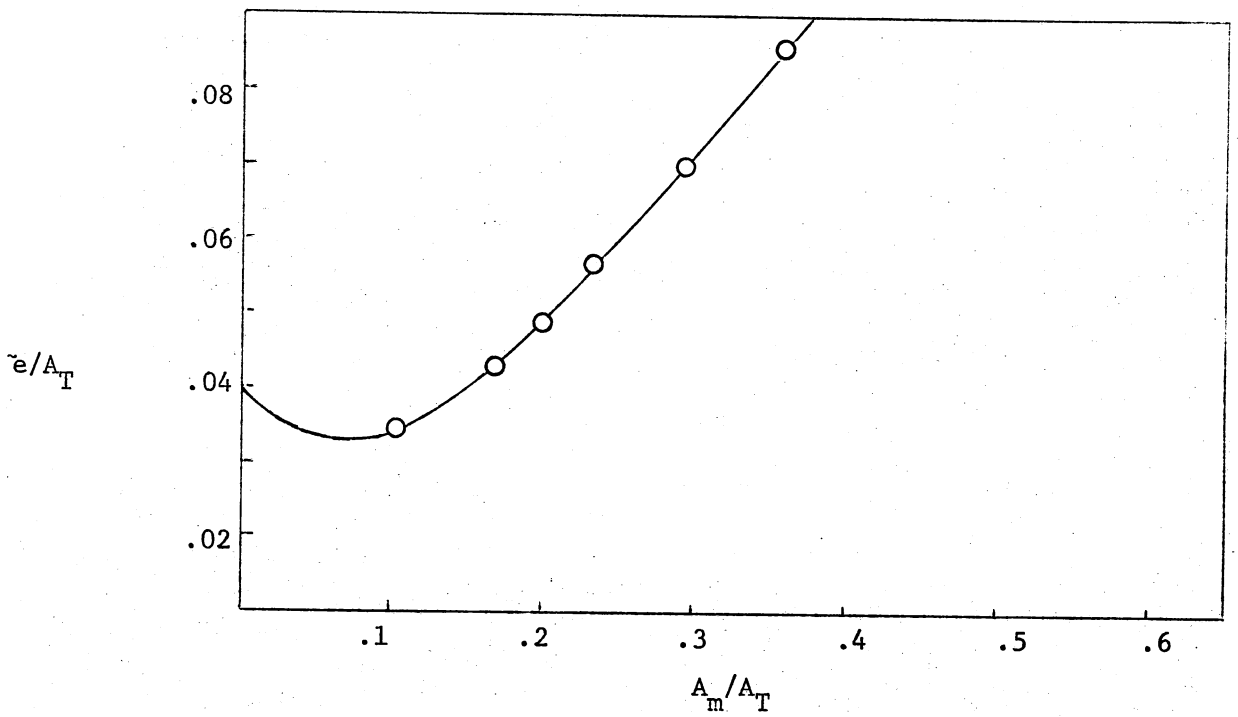

Figure 26. The Resulting Curve Fit in Kovasznay Coordinates for 9/11/75 Data at X/D = 9, on the Shear Layer of the M_j = 2.4 Jet.

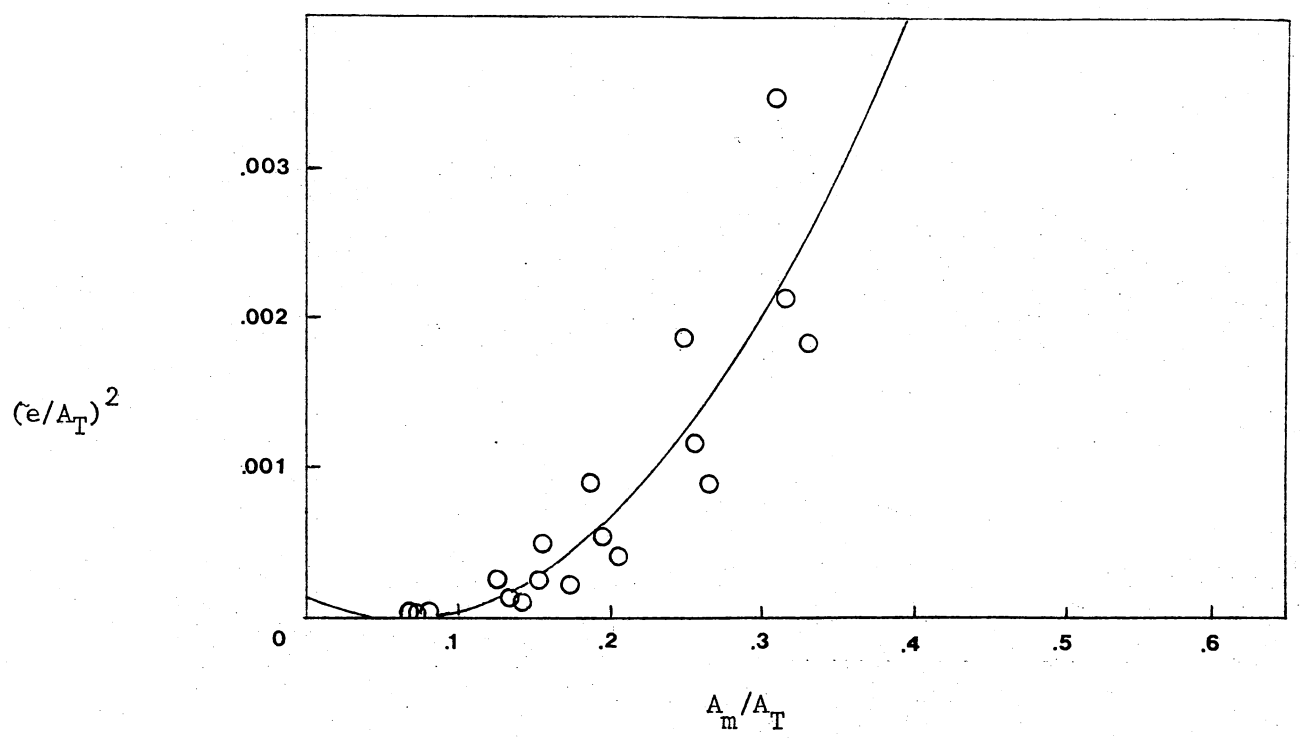

Figure 27. The Second Order Regression Curve Fit for all the CTA Data at X/D = 5, on the Shear Layer of the M_j = 2.4 Jet.

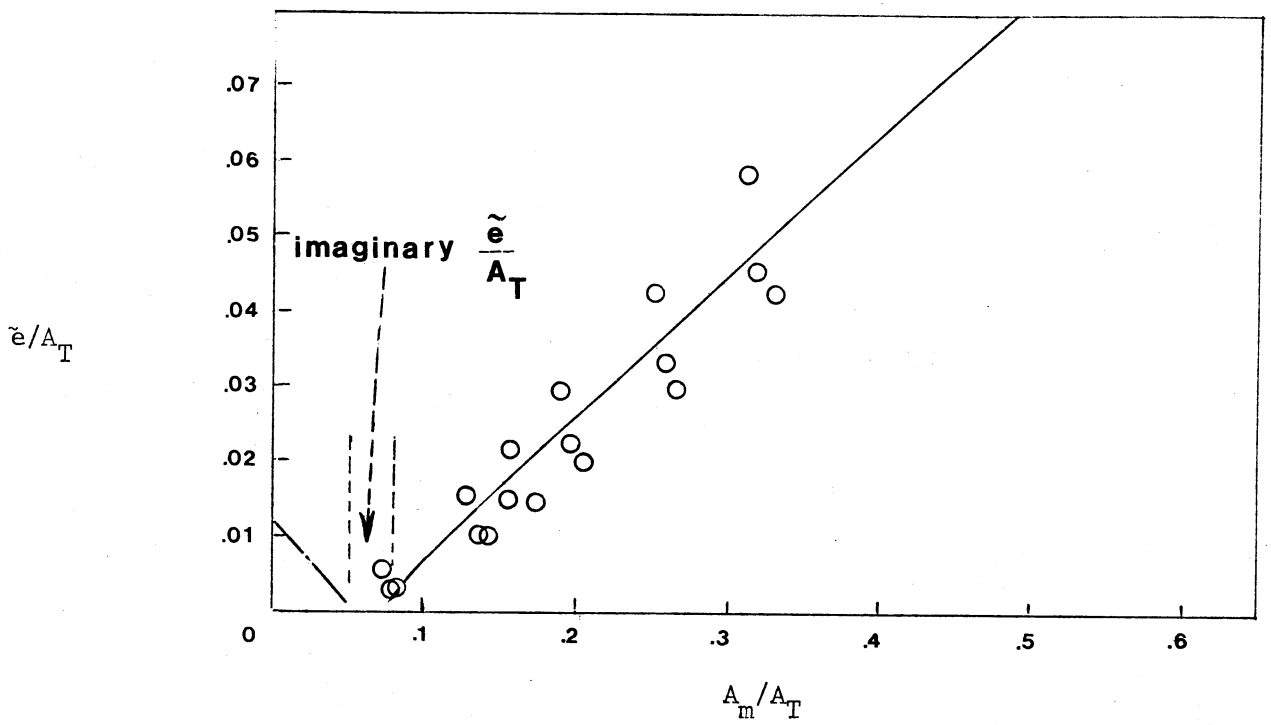

Figure 28. The Resulting Curve Fit in Kovasznay Coordinates for all the CTA Data at X/D = 5, on the Shear Layer of the M_j = 2.4 Jet.

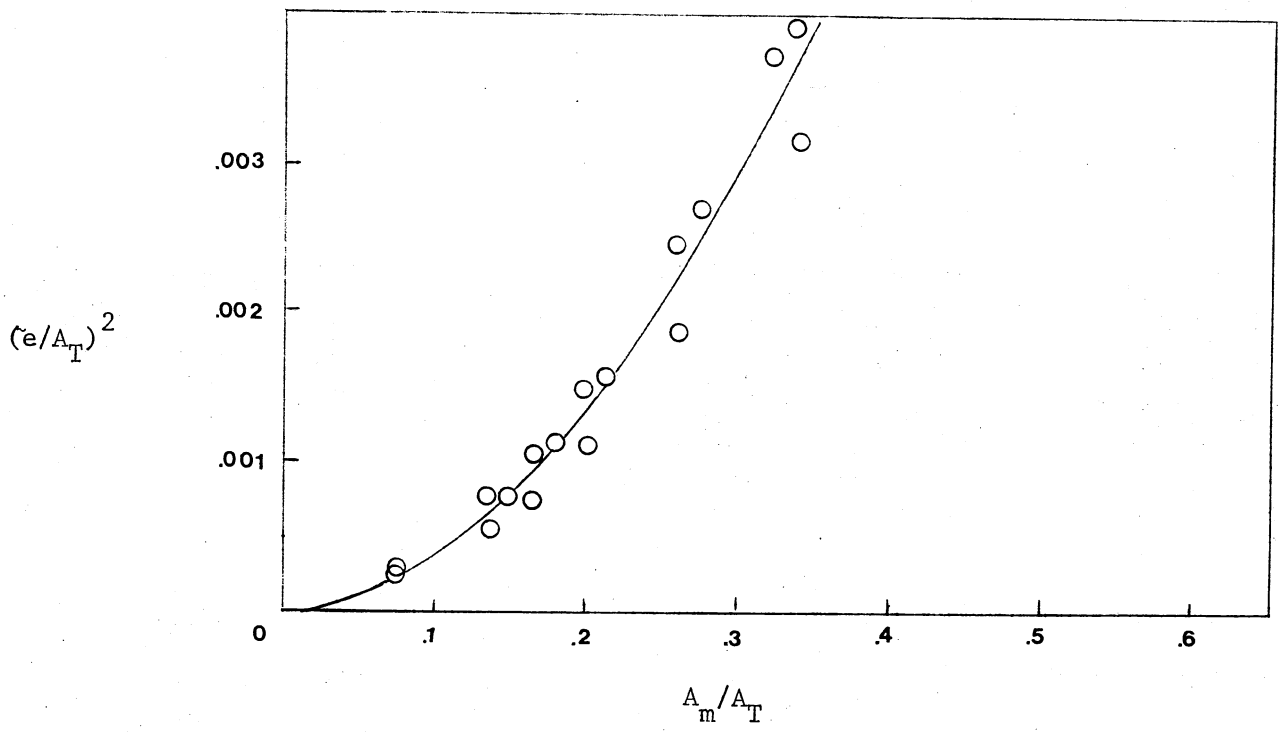

Figure 29. The Second Order Regression Curve Fit of all the CTA Data of X/D = 9, Centerline of the M_j = 2.4 Jet.

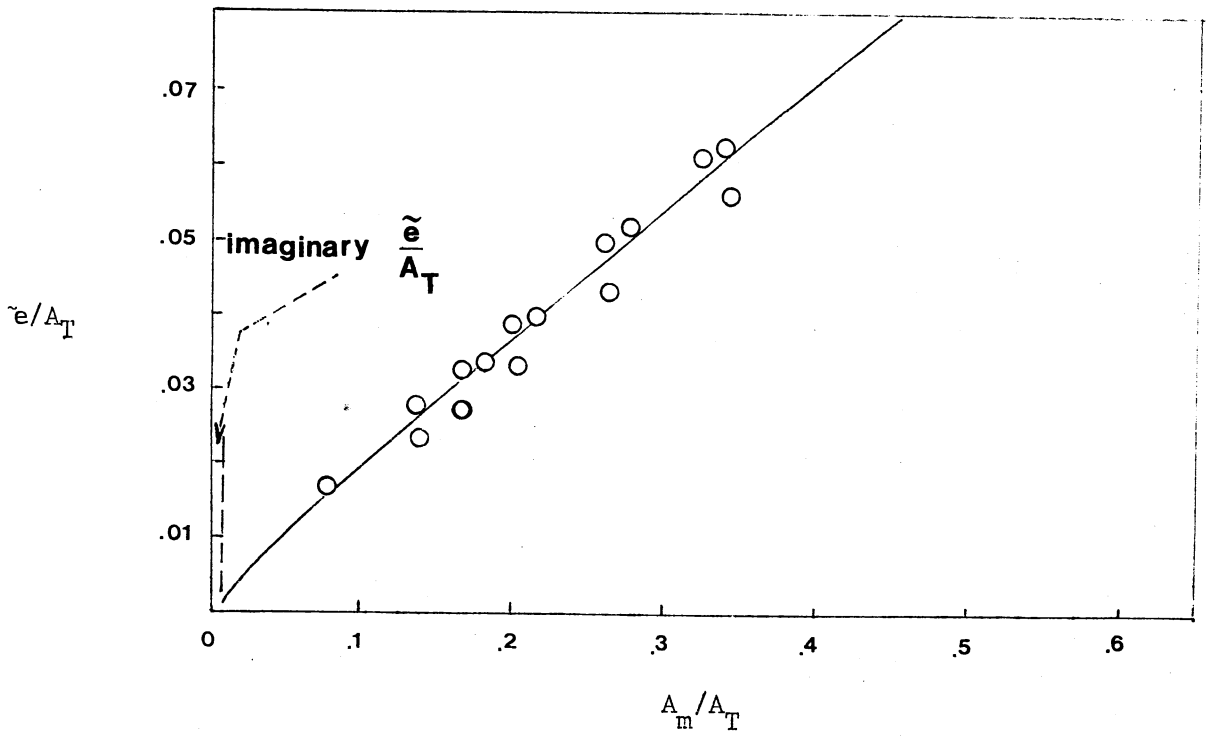

Figure 30. The Resulting Curve Fit in Kovasznay Coordinates for all the CTA Data at X/D = 9, Centerline of the M_j = 2.4 Jet.

VITA

Chin-Long Ko

Candidate for the Degree of

Master of Science

Thesis: IMPROVED TECHNIQUES FOR THE DECOMPOSITION OF HOT-WIRE FLUCTUATION MEASUREMENTS IN SUPERSONIC FLOWS

Major Field: Mechanical Engineering

Biographical:

Personal Data: Born in Taipei, Taiwan, October 17, 1948, the son of Dr. and Mrs. Yuan-Ching Ko.

Education: Graduate from Geng-Kou Junior High School, Taipei, Taiwan, in June, 1963 and Cheng-Kung Senior High School, Taipei, Taiwan, in June, 1966; received Bachelor of Engineering degree in Civil Engineering at Chung Yuan Christian College of Science and Engineering, Chung Li, Taiwan, in June, 1970; received Master of Science degree in Civil Engineering at Oklahoma State University, Stillwater, Oklahoma, in May, 1974; completed requirements for the Master of Science degree in Mechanical Engineering at Oklahoma State University in May, 1976.

Professional Societies: American Institute of Aeronautics and Astronautics, American Society of Mechanical Engineers, associate memeber of National Society of Professional Engineers and the Oklahoma Society of Professional Engineers.